Cellular Network Performance Analysis Under Correlated Shadow Fading

---

DISSERTATION

Submitted in Partial Fulfillment of

the Requirements for

the Degree of

DOCTOR OF PHILOSOPHY (Electrical Engineering)

at the

NEW YORK UNIVERSITY
TANDON SCHOOL OF ENGINEERING

by

Tingting Lu

May 2017

Cellular Network Performance Analysis Under Correlated Shadow Fading

---

DISSERTATION

Submitted in Partial Fulfillment of

the Requirements for

the Degree of

DOCTOR OF PHILOSOPHY (Electrical Engineering)

at the

NEW YORK UNIVERSITY

TANDON SCHOOL OF ENGINEERING

by

Tingting Lu

May 2017

Approved:

_____

Department Chair Signature

_____

Date

University ID: N19324363
Net ID: tl984

Approved by the Guidance Committee:

Major: Electrical Engineering

Shivendra S. Panwar
Professor
Electrical and Computer Engineering

Date

Sundeep Rangan
Associate Professor
Electrical and Computer Engineering

Date

Henry Bertoni
Professor
Electrical and Computer Engineering

Date

Microfilm or copies of this dissertation may be obtained from:

UMI Dissertation Publishing
ProQuest CSA
789 E. Eisenhower Parkway
P.O. Box 1346
Ann Arbor, MI 48106-1346

VITA

Tingting Lu was born ******.

To ******.

ACKNOWLEDGEMENT

First and foremost I would like to thank *******

ABSTRACT

Cellular Network Performance Analysis Under Correlated Shadow Fading

by

Tingting Lu

Advisor: Shivendra S. Panwar

Submitted in Partial Fulfillment of the Requirements for the Degree of Doctor of Philosophy (Electrical Engineering)

May 2017

Due to the severe shortage of capacity in conventional cellular bands, millimeter wave (mmWave) frequency spectrum, between 30 and 300 GHz, has been considered as a key component to addressing the bandwidth needs for next generation networks. The small wavelengths of mmWave will result in high path loss and sensitivity to obstructions which cause large-scale shadow fading. Shadow fading can lead to significant received power loss for a wide area. In reality, shadow fading at two different positions are correlated to each other. Correlated shadow fading downgrades system performance by introducing high outage probability and long-lasting outage duration, which will lead to connection drops. To fully utilize the bandwidth of wireless links, shadow fading needs to be mitigated.

This thesis focuses on discussing the system performance in terms of outage probability and outage duration under correlated shadow fading and developing

efficient ways to mitigate shadow fading, reduce outage probability and provide better Quality of Service (QoS) to users. Starting from the downlink of a single-cell model under distance-angle correlated shadow fading, channel variations due to correlated shadow fading is demonstrated. A cooperative communication solution to reduce the frequency and duration of dropped connections by employing relays is proposed. Secondly, to simplify the analysis, the most commonly used shadowing correlation model: the exponential correlation model, is introduced to investigate the single-cell system. A first-order Markov chain model is developed and validated for exponential correlated shadow fading. Using the proposed Markov chain model, the frequency and duration of outage near the edge of a single cell can be analyzed. This model provides an efficient way to describe the channel variations. Thirdly, the research is expanded to a multi-cell model. Simulations are run to explore the outage probability and outage duration given different Base Station (BS) densities and different deployment models. Increasing BS density is proved to be a valid way to reduce outage probability as long as de-correlation distance is large enough. Meanwhile, increasing BS density will significantly benefit upper layer applications by reducing outage durations. As a next step, we investigate the transport layer after characterizing the physical layer. As a result of the characteristics of mmWave channel, the legacy Transmission Control Protocol (TCP) may not work well for next generation networks. To verify this, the performance of existing TCP on an emulated mmWave channel with periodic on-off behavior is investigated. Simulation results illustrate that existing TCP congestion control algorithms are not optimal for the testing channel. Moreover, those results convinced us that reducing congestion detection time is the key component to developing a proper TCP congestion control protocol for next generation networks. Therefore, we propose a fast end user congestion

detection scheme that has high precision when network topology does not change rapidly.

List of Publications

1. **Tingting Lu**, co-authors, "paper Title," in *Conference name*, Month Year, pp. **.

2. *******

3. *******

Contents

List of Figures

List of Tables

Chapter 1

Introduction

1.1 Challenge, Motivation and Our Approach

The remarkable success of cellular wireless communication technologies makes it possible for smartphones to be widely used, which generates dramatical demand increase for mobile broadband capacity every year [1–3]. As a result, the conventional cellular bands below 3 GHz become very crowded. With the severe shortage of conventional cellular bands, millimeter wave (mmWave), between 30 and 300 GHz, frequency spectrum has been considered as a key component to addressing the bandwidth deficiency in next generation wireless communication networks [4–8]. The available spectrum at these higher frequencies can be easily 200 times as much as today's cellular allocations that are largely constrained to the prime RF under 3 GHz. Moreover, small wavelengths of mmWave signals combined with low-power complementary metal-oxide-semiconductor (CMOS) radio-frequency (RF) circuits enable large numbers of miniaturized antennas to be placed in small dimensions. The usage of these multiple antenna systems makes it possible to make electrically steerable arrays with very high gain to be fabricated

at the Base Station (BS) or even in the cellphone [9–12]. These hardware and system advances promise mmWave a bright future.

1.1.1 Next Generation Cellular Network

There are fundamental differences between the current cellular communication system and the mmWave communication system in terms of high propagation loss and sensitivity to blockage. Applications running on top of the mmWave network require low delay and high capacity. With high capacity, mmWave can easily satisfy the capacity demand. However, fading can substantially affect the performance of a wireless communication system. In general, fading can be divided into two categories: large-scale fading and small-scale fading. Small-scale fading is caused by multipath propagation. Large-scale fading, which is also known as shadow fading, is caused by obstacles in the propagation path. Electromagnetic waves have minimal ability to diffract around obstacle with a size significantly larger than its wavelength. Currently, the frequency used by the LTE system has longer wavelengths than those of mmWave. This makes it possible to overcome the shadow fading caused by small size obstacles. High-frequency mmWave has small wavelengths, which result in sensitivity to blockage caused by small size obstacles like buildings, trees and even nearby pedestrians or vehicles. Therefore, shadow fading can cause significant received power loss and significantly deteriorate the performance of the next generation wireless communication system. MmWave channel can be severely vulnerable to shadowing resulting in outages, rapidly changing channel conditions and intermittent connectivity. Therefore, it is more challenging for mmWave system to provide low delay. According to aforementioned characteristics of mmWave channel, tough challenges need to be solved

in order to fully exploit its potential.

Shadow fading can cause significant received power loss for a wide area. This will lead to lost connections, which is harmful to mobile users who are using real-time applications which require low delay. To fully utilize the high bandwidth of mmWave links, shadow fading needs to be mitigated. Cooperative communication is an efficient way to reduce outage and provide better Quality of Service (QoS) for a single-cell model. Deploying ultra-dense network is considered as an efficient way to mitigate shadow fading for a multi-cell system. In most cases, shadow fading is assumed to be temporally and spatially independent to simplify the analysis of the system performance. Obviously, this is not the real scenario, especially for next generation wireless communication network. For mmWave communication networks, the cell size will become much smaller than current LTE cell size due to high propagation loss [8]. When cell size becomes comparable with the size of obstacles that cause shadow fading, shadow fading cannot be considered as spatially independent. Correlated shadow fading will result in correlated outage events and long outage duration. Consequently, the performance of the system is downgraded in terms of long delay. This thesis focuses on investigating the system performance under correlated shadow fading and proposing methods to mitigate correlated shadow fading. Since there is no consensus on the standard mmWave channel, we discuss the system performance under correlated shadow fading of the legacy cellular spectrum frequency and suggest applying it to mmWave channel in the future.

With non-correlated shadow model, we can only analyze a snapshot of the system. However, in order to predict application performance over time, such as outage durations, correlated shadow fading model is necessary. At first, we choose distance-angle correlation model [13] for shadow fading and investigate the

correlated shadow fading problem in a single-cell cellular network. We find that correlated shadow fading could lead to correlated outage events and long outage durations. To mitigate shadow fading and decrease shadow durations, wireless relays can be deployed. The performance of three different relay deployments with different relay densities is investigated. Theoretical analysis and simulations of outage performance are compared among different relay placement scenarios. The next generation wireless communication networks will be a dense multi-cell network [8], hence single-cell model is not adequate for analyzing next generation wireless communication networks. Interference will affect every receiving channel. Therefore, extending the investigation to a multi-cell network is necessary. When considering a multi-cell system, exponential correlated shadow fading model is used due to its popularity and simplicity.

Exponential correlation model [14] has been widely used by researchers. Considering a single-cell model, exponentially correlated shadow fading can be modeled as a first-order autoregressive process. Given this feature, a first-order Markov chain model is developed and validated to simplify the analysis. The Markov chain model is constructed by partitioning the entire shadow fading range into a finite number of intervals. The state transition matrix of the Markov chain is derived from the joint probability distribution of correlated log-normal shadow fading. Based on the proposed Markov chain model, the frequency and duration of outage near the edge of a single cell can be analyzed. To validate the Markov chain model, correlated Gaussian random fields can be simulated to analyze the outage frequency and durations due to correlated shadow fading. This Markov chain model can not be extended to multi-cell system because of the existence of interference from other base stations (BSs) and the co-existing shadow fading auto-correlation and cross-correlation. To further elaborate the performance of

multi-cell system and mitigate the correlated shadow fading, we run simulations for different BS densities. We believe increasing BS density will improve the system performance under correlated shadow fading. Two scenarios are investigated: MU connecting to the nearest BS and MU connecting to the BS with the strongest signal. We calculate signal-to-noise-and-interference ratio (SINR) for the mobile user (MU) with regard to different scenarios. Outage probability and outage duration can be obtained from the SINR result. We find that increasing BS densities can decrease outage probability when MU is connected to the nearest BS. Outage duration will decrease when increasing the BS density in both cases.

As we have mentioned above, mmWave channel provides a tremendous amount of capacity and relatively low delay while it suffers from high propagation loss and sensitivity to blockage. Simulations and measurements revealed that the capacity gain is significant comparing with current cellular systems in [15, 16]. The last hop wireless channel capacity is not a bottleneck problem anymore. Meanwhile, mmWave channels are prone to variations due to the blockage from walls, trees, or even human body [17–19]. This feature brings frequent capacity variations to the channel. Typically, the channel switches periodically between two states: Line-of-Sight (LOS) and Non-Line-of-Sight (NLOS). The upper layer channel provided by mmWave communication network is not yet standardized; however, in general, there is a consensus that 5G mmWave channel will provide high capacity and low latency with frequent capacity fluctuation. For 5G mmWave wireless communication network, the legacy Transmission Control Protocol (TCP) might not work well due to the slow congestion detection and conservative loss recovery. Therefore, designing a new TCP congestion control scheme without involving any intermediate network device is necessary. In order to investigate existing TCP performance, a GINI testbed based link layer model is employed. This model

is based on an Ethernet channel with high capacity and low delay. We extend the model to allow the physical link to be periodic on-off to mimic the mmWave channel where on means LOS and off denotes NLOS. Existing TCP congestion control protocols are tested on this channel. Both throughputs and the variation of congestion windows are shown with regard to different channel behaviors. A data-driven fast congestion prediction algorithm is proposed based on the idea of Explicit Congestion Notification (ECN). This fast congestion prediction algorithm can be utilized to design next generation transport layer protocols.

1.1.2 Correlated Shadow Fading Models

In most cases, shadow fading is modeled as an independent log-normal distribution [20] with a standard deviation derived from empirical measurements. An independent log-normal shadowing model is used widely when shadow fading cannot be ignored. But this model fails to capture the spatial correlations in shadow fading, which has been proved to be not negligible in [21], [22] and [23]. In [13], the author elaborated several models for correlated shadow fading, investigated their feasibility and presented the physical plausibility of each model. Correlations can be divided into two categories: autocorrelation and cross-correlation as in Figure 1.1. Autocorrelation is the correlation between two receivers receiving signal from the same transmitting node. Cross-correlation considers two transmitting nodes sending data to the same receiver. Autocorrelation and cross-correlation are symmetric in a mathematical sense and can be investigated in the same manner.

Autocorrelation and cross-correlation models can be described as in Figure 1.2. There are N points $Y_1, \cdots, Y_N$. S_i is the logarithm of the power attenuation due to shadowing on each path $\vec{r_i}$. $\mathbb{E}\{S_i\} = 0$ since shadow fading follows correlated

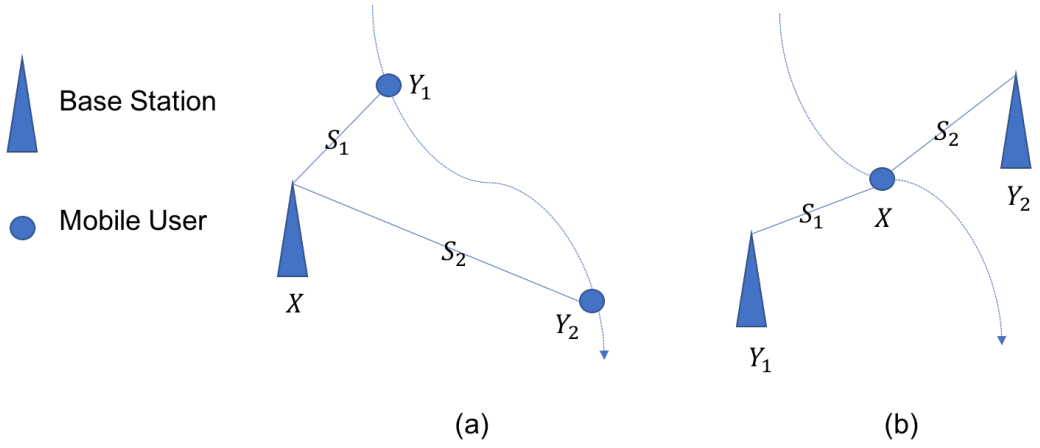

Figure 1.1: (a) Shadowing autocorrelation for a mobile user, (b) Shadowing cross-correlation for a mobile user

log-normal distribution. The log-variance of shadow fading can be characterized as

$$\sigma_i^2 = \mathbb{VAR}\{S_i\} = \sigma_S^2(\vec{r_i}). \tag{1.1}$$

This variance is considered as constant after a certain distance [24].

The correlation coefficients can be defined as

$$\begin{aligned} \rho_{i,j} &= \mathbb{E}\{S_i S_j\}/\sigma_i \sigma_j = h(\vec{r_i}, \vec{r_j}), i \neq j \\ \rho_{i,i} &= 1. \end{aligned} \tag{1.2}$$

The following properties hold:

- $-1 \leq h(\vec{r_i}, \vec{r_j}) \leq 1$
- $h(\vec{r_i}, \vec{r_j}) = h(\vec{r_j}, \vec{r_i})$

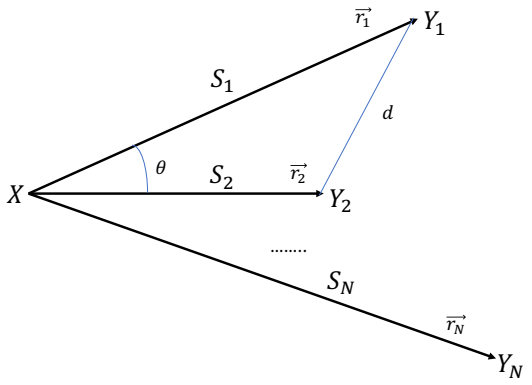

Figure 1.2: Generic geometry of shadowing autocorrelation and cross-correlation

The correlation matrix of $\mathbf{S} = [S_1, \cdots, S_N]$ is:

$$\mathbf{K} = \begin{bmatrix} \sigma_1^2 & \sigma_1\sigma_2\rho_{1,2} & \cdots & \sigma_1\sigma_N\rho_{1,N} \\ \sigma_1\sigma_2\rho_{1,2} & \sigma_2^2 & \cdots & \sigma_2\sigma_N\rho_{2,N} \\ \vdots & \ddots & \ddots & \vdots \\ \sigma_1\sigma_N\rho_{1,N} & \sigma_2\sigma_N\rho_{2,N} & \cdots & \sigma_N^2 \end{bmatrix}. \tag{1.3}$$

For $\mathbf{K}$ to be a valid covariance matrix, it is necessary that $\mathbf{K}$ is positive semidefinite(psd).

By grouping the measurements along one variable in several ways, h can be expressed as a function of a single variable in the following three forms:

- absolute distance (between Y_1 and Y_2): $d = \|\vec{r_1} - \vec{r_2}\|$.
- angle of arrival separation: $\theta = |\angle\vec{r_1} - \angle\vec{r_2}| \in [0°, 180°]$.
- arrival distance ratio (in decibels): $R = |10\log_{10} r_1/r_2| = (10/\ln 10)|\ln r_1 -$

$\ln r_2|$.

A correlation model needs to satisfy as many as the following criteria to become a precise model:

- $h(\vec{r_i}, \vec{r_j}) \approx 1$ for $\vec{r_i} \approx \vec{r_j}$.
- $h(\vec{r_i}, \vec{r_j}) \ll 1$ for $\|\vec{r_i} - \vec{r_j}\| \gg 0$.
- h should be a nonincreasing function in θ, R and d.
- h should be nonnegative.
- h should be small for large θ and approach zero for $\theta \approx 180^\circ$ when r_1 and r_2 are large.
- Continuity: a small change in $\vec{r_i}$ should result in small change in $h(\vec{r_i}, \vec{r_j})$.
- Correlation should not depend on d only.

Considering the above criteria, the author of [13] recommended a correlated shadow fading model with distance and angle in [25], and provided a fast simulation method to generate the correlated shadowing field. We use this model to analyze single-cell system performance and discuss how cooperative communication can help to mitigate shadow fading.

After investigating the single cell system, we attempt to investigate multi-cell system performance. The aforementioned distance-angle model cannot be applied to this scenario. The distance-angle model is designed for single-cell system with a single BS at the center of the shadowing field. Therefore, it is not suitable for multi-cell system. Meanwhile, auto-correlation and cross-correlation co-exist in a multi-cell system, which further complicates the analysis of system performance.

To simplify the analysis without loss of generality, the exponential correlated model is deployed. Exponential correlated model of shadow fading is the most widely used model. It can be modeled as a Markov chain model in the single-cell case. This Markov model can be used to simplify the analysis of system performance; however, it cannot be used to analyze the performance of multi-cell system due to the presence of interference. Simulations are run to study the outage probability and outage duration of the multi-cell system given different network topologies.

1.1.3 Transmission Control Protocol (TCP)

TCP is the transport layer protocol that provides reliable connection-oriented and in-order delivery service to applications [26]. TCP uses error control, flow control and congestion control to achieve this. When incoming traffic demand to the network exceeds its capacity, congestion occurs and propagates to other connected networks. Congestions in the network can generate long delay and high packet loss rate. Due to fading, the mmWave cellular network might be unstable and continuously switching between LOS and NLOS states frequently, thus resulting in large variations in data rate. This behavior determines that mmWave cellular network is prone to congestion. Therefore, designing an efficient congestion control protocol is necessary for next generation wireless communication networks. There are two points to implement congestion control: end-to-end TCP congestion control and queuing discipline in the routers inside the network. In this thesis, we will concentrate on end-to-end TCP congestion control. Legacy TCP uses slow start, congestion avoidance and fast retransmit/fast recovery to adapt to congestion in the routers. The sender maintains two variables for congestion

control: a congestion window size (*cwnd*), which upper bounds the sender rate, and a slow start threshold (*ssthresh*), which determines how the sender rate is increased. Initially, *cwnd* increases exponentially until it reaches *ssthresh*. After that, *cwnd* increases roughly linearly. When congestion occurs, *cwnd* is reduced to 1 segment to avoid segment loss.

TCP relies on implicit signals received from the receiver or the timer times out to learn the state of the network. There are two ways in which TCP can detect packet loss:

- Retransmission timeout (RTO): For each sent TCP segment, the sender expects to receive an acknowledgement (ACK) from the receiver within some period of time (RTO). If the ACK to a particular segment is not received by the sender before retransmission timer expires, the segment is considered to be lost.

- Duplicate ACKs: If the receiver received out of order data segment, it cannot acknowledge the out of order segment. Instead, it will acknowledge the last contiguous segment it has received prior to the lost segment. Upon the reception of the duplicate ACKs, the sender is informed about the loss of the segment.

Both methods above require the sender to wait for a period of time before initiating retransmission (RTO or duplicate ACKs).

Considering characteristics of the mmWave channel, legacy TCP is not necessary a good choice for next generation networks. TCP works for regular network, which is stable and the only variation is congestion. However, it will not work well with mmWave channel, which has an on-off behavior and result in lots of packet loss. The slow start will be too conservative for senders to fully utilize

the channel capacity. Since low delay mmWave channel switches between LOS and NLOS fast and frequently, time out and duplicate ACKs might not indicate the network condition precisely due to the long waiting time. To investigate the existing TCP performance on the mmWave-like channel, we used high-capacity Ethernet channel with periodical on-off behavior to mimic the mmWave channel. TCP throughput of NewReno and Cubic [27, 28] is tested on this channel.

There are also some non-TCP congestion control techniques including Random Early Detection (RED) [29], Explicit Congestion Notification (ECN) [30] and so on. After investigating the legacy TCP performance on a mimic mmWave channel, we propose an end-user TCP congestion prediction algorithm based on ECN. The key idea of ECN is to mark packets as congestion experienced when the routing queue is longer than a threshold instead of dropping them. When the receiver receives the marked packet, it responses with a marked ACK to inform the sender that congestion may occur in the router. TCP senders can adjust their rate of transmission based on their own congestion avoidance algorithm. Inspired by ECN, we propose a data driven virtual ECN algorithm to predict network congestions without involving routers or receivers.

1.2 Dissertation Outline

This thesis is organized as follows. In Chapter 2, we introduce the distance-angle correlated shadow fading model and investigate the system performance of a single cell cellular network. We explain that the correlated shadow fading could lead to correlated outage events and long outage durations. To mitigate the shadow fading, relays are deployed to work cooperatively with the BS. The performance of three different relay deployments with different relay densities are

discussed. Theoretical analysis and simulations of outage performance are given to compare between different relay placement scenarios.

In Chapter 3, the most widely used shadow fading correlation model: exponential correlation model is introduced. A Markov chain model is constructed for the spatially exponentially correlated shadow fading. This model can be used to analyze the outage behavior for a single-cell system. We demonstrated that a well designed Markov chain model with an appropriate number of states corresponding to the standard deviation of the shadow fading is indeed a powerful tool to study system performance.

In Chapter 4, we extend the system performance analysis under exponentially correlated shadow fading from a single-cell system to a multi-cell system. We compare two different BS layout: Grid and Random model, and conclude that Grid model performs better than Random model. System performance is investigated in terms of outage probability and outage duration given different BS densities and connection strategies.

In Chapter 5, we investigate the performance of legacy TCP on a mimic mmWave channel. Results suggest that legacy TCP is not well designed for next generation networks. We propose a data driven machine learning congestion detection algorithm, which can predict network congestion with high precision when network topology does not change dramatically. In the future, a fast reacting congestion control algorithm can be designed based on this algorithm.

Chapter 6 concludes the thesis and discusses some future research directions.

Chapter 2

Mitigate Correlated Shadow Fading by Cooperative Relay Communication

In a cellular network, connections between the Base Station (BS) and Mobile Stations (MS) may fail when the channel is in a deep fade. Shadow fading is large-scale fading which can cause significant received power loss for a wide area. This will lead to lost connections and/or packet loss which is harmful to mobile users, especially to those who are using real-time applications such as video conferencing. Cooperative communication is an efficient way to reduce outage and provide better Quality of Service (QoS) support for delay sensitive applications. A third station, which is often referred as a relay, can be used to forward signals between the BS and the MS. This chapter focuses on a study of the performance of relay deployments under correlated shadow fading. We consider the downlink direction in a single cell deployment, for which the shadowing effect is modeled as an angle and distance based correlated shadowing. The received signal-to-noise ratio

(SNR) is then calculated by assuming jointly Gaussian shadow fading at the MS. Simulation results show channel variations over time with fixed user speed under different relay deployments. These results demonstrate that a modest number of relays can improve the performance of real-time applications significantly.

2.1 Background

In a cellular communication system, the connection between the base station and a mobile station may be dropped when the mobile enters a deeply shadowed area. Shadow fading due to buildings, mountains or even trees significantly reduces the power of the received signal. In most cases, shadow fading is assumed to be temporally and spatially independent [31]. In [32] and [33], the effects of correlated shadowing in connectivity is demonstrated, which indicates that reliable connectivity will be much more difficult to maintain than indicated by independent fading shadow models. In a cellular system, for a downlink, the transmitter is a Base Station (BS) and the receiver is a Mobile Station (MS). For real-time applications (e.g. video conferencing), which require high bandwidth and are delay sensitive, the session may get dropped. In general, within a speed limit, the faster the MS moves, the more frequently the channel condition changes and the higher the connection loss frequency. The focus of this chapter is to study channel variations due to correlated shadow fading, and provide a solution to reduce the frequency and duration of dropped connections by employing relays when the MS is moving.

Cooperative communication has been proven to be an efficient way to mitigate fast fading and increase the robustness of data connections [34,35]. However, cooperative communication can also efficiently maintain the connection whenever

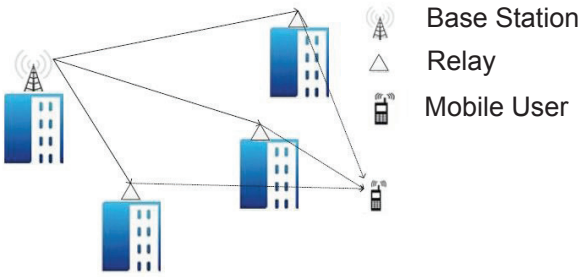

Figure 2.1: Cooperative Communication Example.

the channel condition experiences a sudden deterioration due to shadow fading by switching to different relays. Figure 2.1 is an example of cooperative communication where relays and BS are placed on the top of buildings. In this case, when the MS moves to the area behind a tall building, with a high probability the signal transmitted from the BS will be obstructed by the building, and consequently the MS will encounter deep shadow fading. The channel between BS and MS will degrade and data rate will drop suddenly. In the worst case scenario, the connection with the BS may be totally lost. To combat this effect and enhance the signal received by the MS in this case, relays can be deployed on the top of tall buildings to relay the signals from the BS to MS to maintain good channel conditions between the BS and MS.

Cooperative communication has been a topic of research for several years. Madan et al. [36] studied multi-user spatial diversity in a shadow-fading environment. Other work [37–39], studied relay selection and cooperative relaying over different fading channels in different systems. Patwari et al. [40] studied relay placement in realistic deployments and confirmed that Rayleigh fading alone is not an appropriate assumption for evaluating network performance in a real deployment. In [41, 42], the authors analyzed outage probability and its duration with cooperative relaying. In an 4G-LTE network, which is strongly resilient to

multipath fading, shadow fading becomes the most important fading factor [31]. Given the presence of relays, the channel variation experienced by an MS in an environment with correlated shadow fading is still an open problem. In this chapter, we analyze this problem in a single cell, and give insights on how relays could mitigate shadow fading. We will derive the critical relay density that can guarantee a certain QoS between the BS and an MS.

In most cases, shadow fading is modeled as an independent log-normal distribution [20] with a standard deviation derived from empirical measurements. An independent log-normal shadowing model is used widely when shadow fading cannot be ignored. In the log-normal shadowing model, the path loss ψ is assumed random, with a log-normal distribution given by

$$p(\psi) = \frac{\xi}{\sqrt{2\pi}\sigma_{\psi_{dB}}\psi} exp[-\frac{(10\log_{10}\psi - \mu_{\psi_{dB}})^2}{2\sigma^2_{\psi_{dB}}}], \psi > 0, \tag{2.1}$$

where $\xi = 10/\ln 10$, $\mu_{\psi_{dB}}$ is the mean of $\psi_{dB} = 10\log_{10}\psi$ and $\sigma_{\psi_{dB}}$ is the standard deviation of ψ_{dB}. The distribution of the dB value of ψ is Gaussian with mean $\mu_{\psi_{dB}}$, standard deviation $\sigma_{\psi_{dB}}$ and is given by:

$$p(\psi_{dB}) = \frac{1}{\sqrt{2\pi}\sigma_{\psi_{dB}}} exp[-\frac{(\psi_{dB} - \mu_{\psi_{dB})^2}}{2\sigma^2_{\psi_{dB}}}]. \tag{2.2}$$

The above model fails to capture the spatial correlations in shadow fading. Empirical measurements show that shadowing has significant correlations in realistic scenarios that can affect system performance [21]. Considering the distribution of obstructions and the speed of the MS, a realistic channel propagation model should incorporate correlated shadow fading. Szyszkowicz et al. [13] presented a review and analysis of the feasibility of different correlated shadowing models.

In cooperative communications, relays help the BS to maintain the connection with the MS. Different cooperative schemes can be used by relays. Typically there are two schemes: Amplify-and-Forward (AF), Decode-and-Forward (DF) [43]. In the AF mode, relays amplify the noisy signal received from the source and forward to the MS. In the DF mode, relays decode the signal received from the BS, then encode it and forward the coded signals to the MS. In this chapter, we assume that DF scheme is used by relays.

Given a fixed placement of BS and a fixed moving trajectory for the MS, the efficient placement of relays to maintain the connection between BS and MS and the resulting reduction of the MS's outage probability under correlated shadow fading is the main focus of this chapter. The key contributions of this chapter are summarized below.

- An analysis of the relationship between correlated shadow fading and correlated outage events.
- Show how relays help mitigate correlated shadow fading. Correlated outage fields with and without relaying are given and compared.
- Analyze the performance of three different relay deployment schemes with different relay densities. The performance includes computing the best channel gain and the resulting change in outage probabilities. We also compare the advantages and disadvantages of different relay deployments.

The chapter is organized as follows: Section 2.2 presents the correlated shadow fading model that is used in this chapter and the resultant correlated outage. Section 2.3 presents the system model with three different relay deployments. Section 2.4 gives theoretical analysis of how relays mitigate shadow fading and

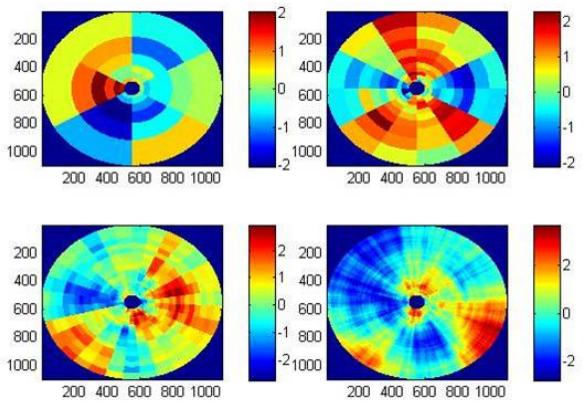

Figure 2.2: Correlated Shadowing Fields for Increasing Resolutions (The disk area is the generated correlated shadowing field and the color of the areas refers to the normalized standard deviation which is $S_i/\sigma_s(\vec{r_i})$)

reduce outage probability. Section 2.5 presents the simulation setup and analyzes the simulation results of different relay deployments. Section 2.6 summarizes the chapter.

2.2 Correlated Shadow Fading

As stated in the introduction, empirical measurements show that there exist different patterns of correlations between the shadowing. The independent log-normal shadow fading model, while very useful for static MS performance analysis, cannot reflect the correlation of shadow fading between different locations. In this section, we will give a brief introduction of shadow fading models, including the model used in this chapter. There is no single mathematical model which captures all different categories of correlation [13]. In this chapter, we use the correlated shadow fading model which incorporates the angular and distance correlations of shadow fading [25]. In [25], the author states that correlation in shadowing is indispensable for the analysis of interference of large networks and gives a time-

efficient fast shadowing fields generation algorithm. The algorithm generates a correlated shadowing field $\vec{S}$, which gives shadow fading factor $\vec{s_i}$ for each path $\vec{r_i}$ with a correlation matrix

$$\mathbf{K}_{N\times N} = [\sigma_s(\vec{r_i})\sigma_s(\vec{r_j})h(\vec{r_i}\vec{r_j})], \tag{2.3}$$

where N paths interfere with path $\vec{r_i}$ and $\mathbf{E}\{S_i^2|\vec{r_i}\} = \sigma_s^2(\vec{r_i})$. This model assumes that in the correlation matrix, h is separable with respect to the angle of arrival

$$\theta = |\angle\vec{r_i} - \angle\vec{r_j}| \in [0^\circ, 180^\circ], \tag{2.4}$$

and the arrival distance ratio

$$R = |10\log_{10} r_i/r_j| = \frac{10}{\ln 10}|\ln r_i - \ln r_j|, \tag{2.5}$$

$$h(\vec{r_i}, \vec{r_j}) = max\{1 - \theta/\theta_0, 0\} \cdot max\{1 - R/R_0, 0\}. \tag{2.6}$$

Following the fast shadowing field generation algorithm, we generate shadowing fields with different values of tunable parameters. The shadowing fields are shown in Figure 2.2 with increasing resolutions. Four circular correlated shadowing fields are generated. The shadowing fields are similar to those generated in [25].

2.2.1 Correlated Outage Field

Given a correlated shadowing field, the outage events at different locations are also correlated. Here we analyze correlated outage events under correlated shadow fading and later give an example. In the spatial correlation of outage events, without considering Rayleigh fading, path loss is considered as constant

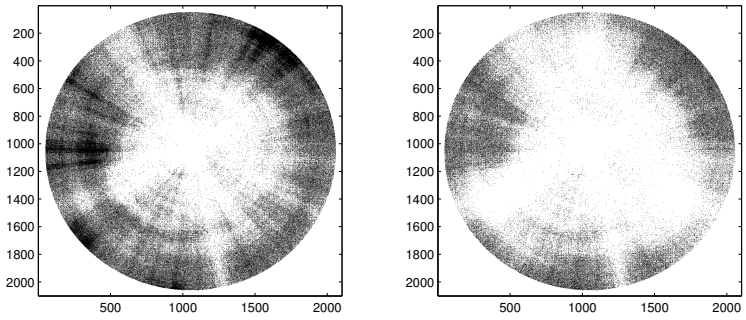

Figure 2.3: Correlated Outage Fields (Dark areas are outage areas while white areas are non-outage areas)

at a fixed time point. Based on the correlated shadowing field we can generate a correlated outage field. Let G denotes total channel gain, PL denotes path loss, and S denotes shadow fading factor, we then have:

$$G = PL * S. \tag{2.7}$$

For two different positions, the correlation coefficient of the two total channel gains is of the following form:

$$\rho_{1,2} = \frac{E[G_1 G_2]}{\sqrt{(Var(G_1)Var(G_2))}}, \tag{2.8}$$

where $G_1 = PL_1 * S_1$ and $G_2 = PL_2 * S_2$. At a fixed time point, temporal correlation is neglected and only spatial correlation is considered, then PL_1, PL_2 can be assumed to be constants, which means that $E[PL_1] = PL_1$, $E[PL_2] = PL_2$. Based on this assumption, we have

$$E[G_1 G_2] = PL_1 PL_2 E[S_1 S_2], \tag{2.9}$$

$$Var(G_1) = PL_1^2 Var(S_1), \tag{2.10}$$

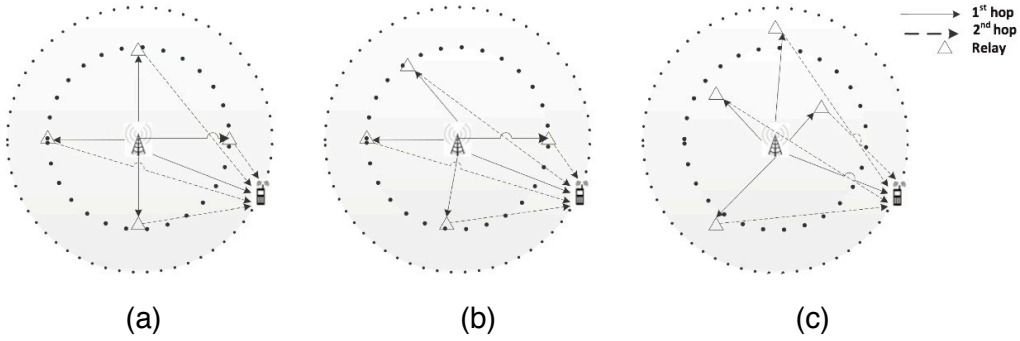

Figure 2.4: System Model and Three Different Relay Placements

$$Var(G_2) = PL_2^2 Var(S_2). \tag{2.11}$$

Based on (2.9), (2.10) and (2.11), it is straightforward to rewrite (2.8) as:

$$\rho_{1,2} = \frac{E[S_1 S_2]}{\sqrt{Var(S_1)Var(S_2)}} = \rho_{S_1,S_2}. \tag{2.12}$$

The channel gain has a spatial correlation coefficient as shown above. Based on the result above, a correlated channel gain field can be generated. Given a proper threshold γ, the correlated outage field can be generated as in Figure 2.3. On the left, a correlated outage field without relaying is shown while the correlated outage field with relaying (3 relays uniformly placed on a circle near the edge) is given on the right. The black color indicates outage areas. In the next section we will present the methodology that helped us generate the results with relays.

2.3 System Model

Since most of the key aspects of the problem can be studied in a single cell, we consider a single cell cellular deployment, where the BS is located at the center of the cell. Figure 2.4 shows the system model that is used in this chapter. Several

relays are placed in the cell and an MS is moving at a particular speed along the circumference at the cell edge. We picked this trajectory since it is the most challenging path given the combination of shadowing and path loss. We consider three relay deployment modes. From left to right in Figure 2.4, (a) is the mode where relays are placed uniformly on a circle near the cell edge; (b) is relays that are randomly spaced on a circle near the cell edge; (c) is relays placed randomly in the cell. By varying relay densities in the above three different models we can analyze which combination of relay density and relay placement can meet the required QoS.

2.3.1 Cooperative Communication Scheme

In this system, the BS and relays work cooperatively to try to guarantee that the MS has sufficient received power either from the BS or from relays with high probability. There are two main cooperative communication schemes: Amplify-and-Forward, and Decode-and-Forward. In this chapter, we assume that relays use the Decode-and-Forward scheme. The cooperative communication system works in the following manner:

- First Hop: BS broadcasts signals to both relays and MS. If MS receives and decodes the signals transmitted by the BS successfully, there is no need for relays to repeat the transmission. If not, relays which successfully decode the signals will participate in the second hop retransmission. This mode of operation will require some signaling overhead, which is not addressed in this chapter. Relays which cannot decode the received signal successfully, will not participate in the second hop.

- Second Hop: Among all relays which participate in the second hop, the one

that has the best channel gain between the relay and MS will be chosen (this can be done by centralized control or using information from pilot signals). This relay will encode the signals again and send the coded bits to the MS.

The received signal in a link ($S \rightarrow D$) between the source and destination is given by:

$$y_D = G_{SD} x_S + n_D, \tag{2.13}$$

where x_S is the signal transmitted by the source and y_D is the signal received by the destination. $n_D \sim \mathcal{CN}(0, N_0)$ is additive white Gaussian noise. G_{SD} is the channel gain from source to destination including path loss and shadow fading. $\text{SNR} \triangleq P * G_{SD}^2 / N_0$, is the end-to-end received signal-to-noise ratio (SNR) and P is the transmitted power. The destination successfully receives the signals if no outage event happens, i.e., $\log_2(1 + \text{SNR}) \geq R$, where R is the required data rate. From the definition of SNR, no outage event happens as long as $\text{SNR} > \gamma$, where $\gamma = 2^R - 1$. In the first hop, relays that can successfully decode the signals transmitted from the BS is a subset $\mathcal{R}_n$ of N relays defined by:

$$\mathcal{R}_n \triangleq \{i : \log_2(1 + \text{SNR}_{S-i}) \geq R\}, \tag{2.14}$$

where SNR_{S-i} is the received signal-to-noise ratio from BS to relay i and $n \in \{0, 1, \cdots, 2^N\}$. In the first hop, the relay can successfully decode the BS signals if $\text{SNR}_{S-i} > \gamma$. The indices of all relays which are able to successfully decode BS signals form a set $\mathcal{R}_n$. In the second hop, the selected best relay j is the relay in $\mathcal{R}_n$ that has the maximum SNR among all relays in $\mathcal{R}_n$, i.e., $j = \arg\max_{i \in \mathcal{R}_n} \{\text{SNR}_{i-D}\}$, where SNR_{i-D} denotes the SNR from the ith relay to the destination MS. The BS to MS SNR is denoted by SNR_{S-D}. The SNR is

determined by distance related path loss and large-scale correlated shadow fading.

2.4 Outage Probability Analysis

Due to the variations of the channel gain caused by shadow fading and path loss of the propagation environment, if the end-to-end channel capacity is below the transmission rate, an outage occurs and the information packets are lost. The outage probability is an important performance measurement of the communication system. In this section, the expression for outage probability is derived.

2.4.1 Outage Probability of the Cooperative Communication System

If an MS cannot directly receive the signal from the BS and none of the relays can decode the BS signal, or if the MS has a bad channel with all relays which successfully decode the BS signal, then an outage event will take place. The probability that an MS cannot receive signals directly from the BS successfully is given below:

$$P_{out_0} = P[\mathrm{SNR}_{S-D} < \gamma]. \tag{2.15}$$

Under the assumption that an MS cannot successfully receive signals from the BS, the outage event happens in the first hop if no relay can receive the signal from the BS successfully, which means $\mathcal{R}_0 = \phi$. Based on this assumption we have:

$$P_{out_1} = \max_{i=1,\cdots,N} P[\mathrm{SNR}_{S-i} < \gamma]. \tag{2.16}$$

If the outage does not happen in the first hop, then the outage event may happen in the second hop with probability:

$$P_{out_2} = \sum_{n=1,\cdots,2^N} P[\mathrm{SNR}_{j-D} < \gamma | \mathcal{R}_n] P[\mathcal{R}_n], \tag{2.17}$$

where j is the index of the relay which has the best channel gain between it and the MS. So the outage probability of the system is

$$P_{out_S} = P_{out_0} * (P_{out_1} + (1 - P_{out_1}) * P_{out_2}). \tag{2.18}$$

The probability density function (pdf) of shadow fading S given L correlated fading branches is

$$\begin{aligned} f_{\mathbf{S}}(\mathbf{s}) = & \frac{\lambda^L}{\sqrt{2\pi}|\mathbf{K}_{L\times L}|^{1/2}\prod_{i=1}^{L} s_i} \\ & \cdot \exp(-\frac{1}{2}(10\log_{10}\mathbf{s} - \boldsymbol{\mu})^T \mathbf{K}_{L\times L}^{-1}(10\log_{10}\mathbf{s} - \boldsymbol{\mu})), \end{aligned} \tag{2.19}$$

where $\lambda = 10/\ln 10$ and $\boldsymbol{\mu}$ is the average shadow fading which is normally 0. $\mathbf{K}_{L\times L}$ is the correlation matrix which is defined in (2.3). Let $\theta_i = \frac{10\log_{10} s_i - \mu_i}{\sqrt{2}\sigma_i}$, and doing a change of variables gives us the pdf of $\boldsymbol{\Theta}$ as follows:

$$f_{\boldsymbol{\Theta}}(\boldsymbol{\theta}) = \frac{1}{\pi^(L/2)|\boldsymbol{\Sigma}|^{1/2}} \exp(-\boldsymbol{\Theta}^T \boldsymbol{\Sigma}^{-1} \boldsymbol{\Theta}), \tag{2.20}$$

where $\boldsymbol{\Sigma}$ is the correlation coefficient matrix which is

$$\begin{bmatrix} 1 & h_{1,2} & \cdots & h_{1,L} \\ \vdots & \ddots & \ddots & \vdots \\ h_{L,1} & h_{L,2} & \cdots & 1 \end{bmatrix}. \tag{2.21}$$

Since SNR $= PL + S - N_0$ in dB, SNR$> \gamma$ means $S > \gamma - PL + N_0$. Given $\mathcal{S}_0 = \phi$, and letting γ_{ai} denote the shadow fading threshold for the ith relay in the ath hop and where $a = 0, 1, 2$, where the 0th hop is the direct transmission from BS to MS, we then have

$$P_{out_1} = \underbrace{\int_{-\infty}^{+\infty} \cdots \int_{-\infty}^{+\infty}}_{i=1,\cdots,N} \prod g_0(\gamma_{1i}) f(\mathbf{s_1}) d\mathbf{s_1}. \tag{2.22}$$

For $n = 1, \cdots, 2^N$, the outage probability for the second hop is

$$\begin{aligned} P_{out_2} = \sum_{n=1,\cdots,2^N} & \underbrace{\int_{-\infty}^{+\infty} \cdots \int_{-\infty}^{+\infty}}_{i=1,\cdots,N} \prod g_n(\gamma_{1i}) f(\mathbf{s_1}) d\mathbf{s_1} \\ & \cdot \underbrace{\int_{-\infty}^{+\infty} \cdots \int_{-\infty}^{+\infty}}_{i \in \mathcal{R}_n} \prod g_n(\gamma_{2i}) f(\mathbf{s_2}) d\mathbf{s_2}, \end{aligned} \tag{2.23}$$

where $\mathbf{s_1}$ is the correlated shadow fading in the first hop, $\mathbf{s_2}$ is the correlated shadow fading in the second hop, u is a step function and

$$g_n(\gamma_{ai}) = \{ \begin{array}{ll} u(\gamma_{ai}) & i \in \mathcal{R}_n \\ 1 - u(\gamma_{ai}) & i \notin \mathcal{R}_n \end{array}. \tag{2.24}$$

Due to the random nature of propagation environment, P_{out_0} is beyond our control. Therefore, to reduce the outage probability, we need to reduce P_{out_1} and P_{out_2}. Relays at proper positions with sufficient density can reduce the outage probability. Comparing different relay placements and finding the appropriate relay density to guarantee the outage probability requirement is the main issue that we will consider next.

2.5 Simulation and Performance Evaluation

To study which relay placement yields the best system performance i.e., the lowest outage probability for continuous real-time applications that we assume to be running on an MS moving at the cell edge (for the given cooperative communication scheme), we set up simulations and compare performance for different relay placements.

2.5.1 Relay Placement

Different relay placements as shown in Figure 2.4 are studied and compared in this section.

- Mode 1: Relays are uniformly spaced on a circle near the cell edge.
- Mode 2: Relays are randomly spaced on a circle near the cell edge.
- Mode 3: Relays are randomly placed in the cell.

2.5.2 Simulation Configuration

In this chapter, the Okumura-Hata model [44] is used to estimate the path loss. The values of parameters that are used in the simulation are shown in Table 2.1. In Mode 1 and Mode 2, the radius of the circle where relays are placed (near the edge) is $700m$.

2.5.3 Simulation Results and Analysis

In this section, numerical analysis and simulation results are presented. The best channel condition that the user can get from either BS or relay is simulated to demonstrate the improvement of the received signal strength at the MS.

Table 2.1: Simulation Configuration Parameters

Okumura-Hata Model	BS Height: $100m$ Relay Height: $10m$ MS Height: $1.5m$
Correlated Shadow Fading	$R_0 : 6$ $\theta_0 : \pi/3$ $d_{min} : 50m$
Relay Placements	Three Modes with Density: 2,4,6,8,10,12
Cell Size	$R : 1000m$
MS Moving Speed	$v : 10m/s$
Radio Frequency	$f : 900MHz$
BS Transmission Power	$P : 26dbm$
SNR Requirement	$8dB$

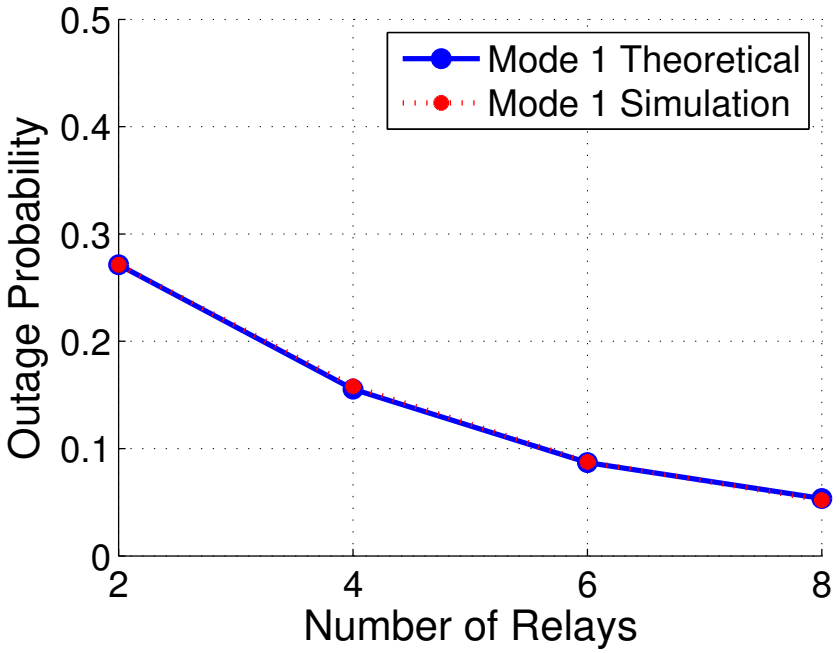

Figure 2.5: Theoretical and Simulated Outage Probability for Mode 1.

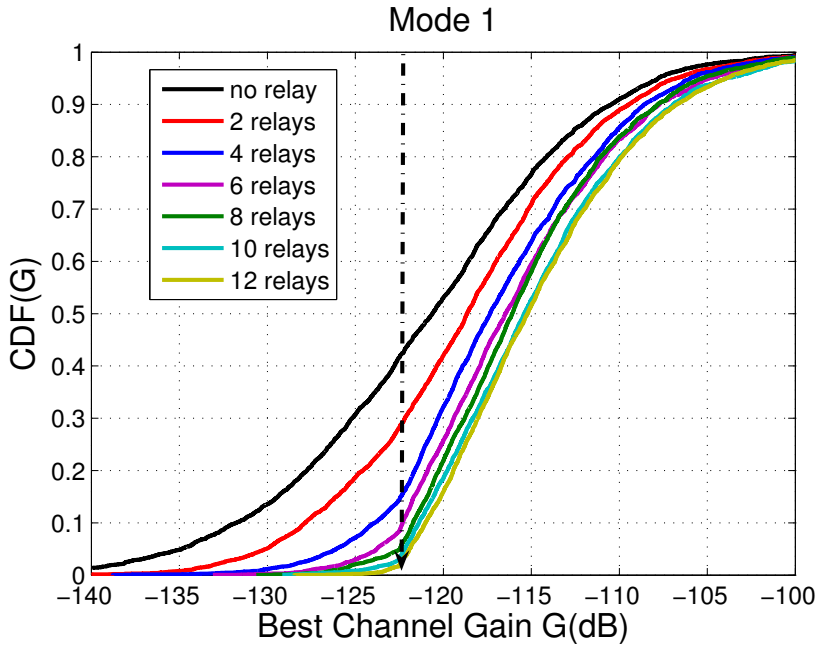

Figure 2.6: Best Channel Condition between MS and BS or Relays of Mode 1 (Dashed arrow demonstrates the channel condition that satisfies the SNR requirement)

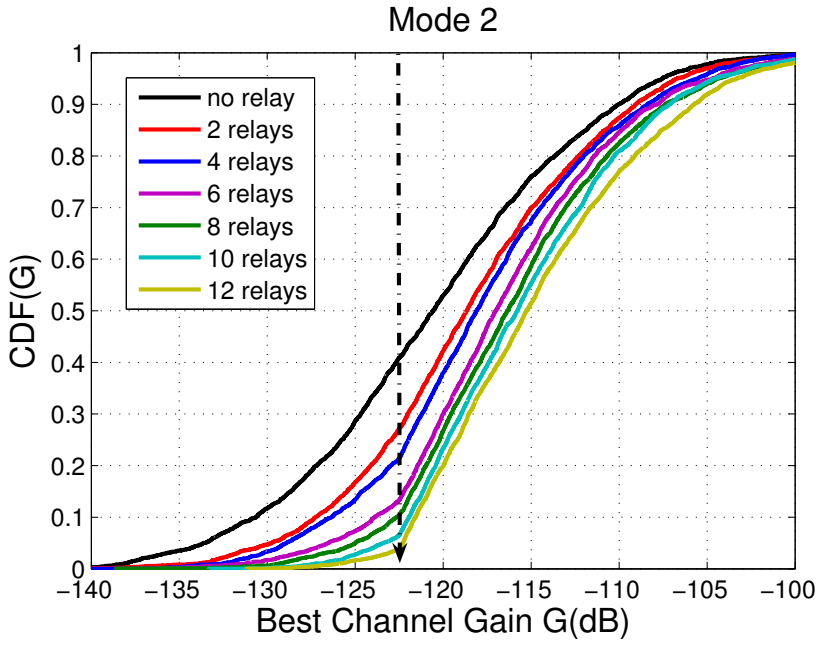

Figure 2.7: Best Channel Condition between MS and BS or Relays of Mode 2 (Dashed arrow demonstrates the channel condition that satisfies the SNR requirement)

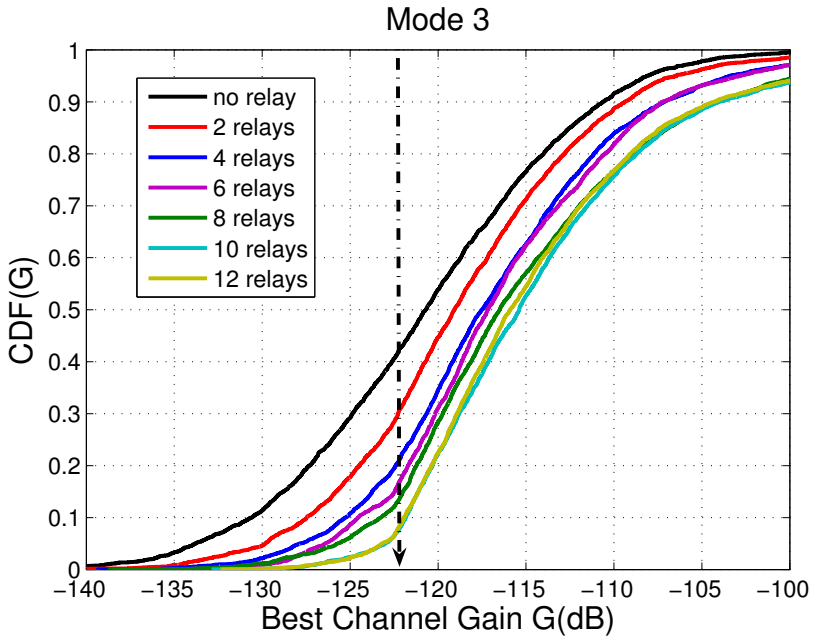

Figure 2.8: Best Channel Condition between MS and BS or Relays of Mode 3 (Dashed arrow demonstrates the channel condition that satisfies the SNR requirement)

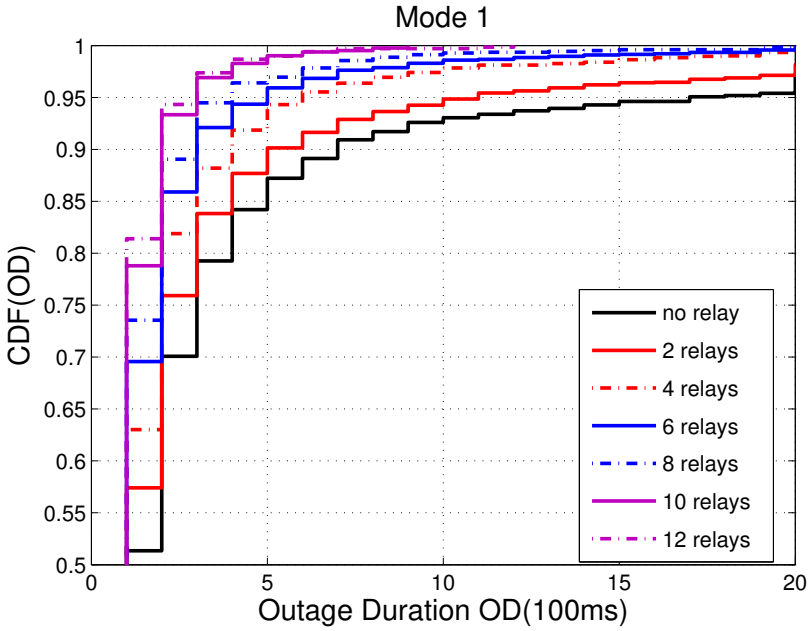

Figure 2.9: Cumulative Distribution Function of Outage Duration of Mode 1 (with Rayleigh fading)

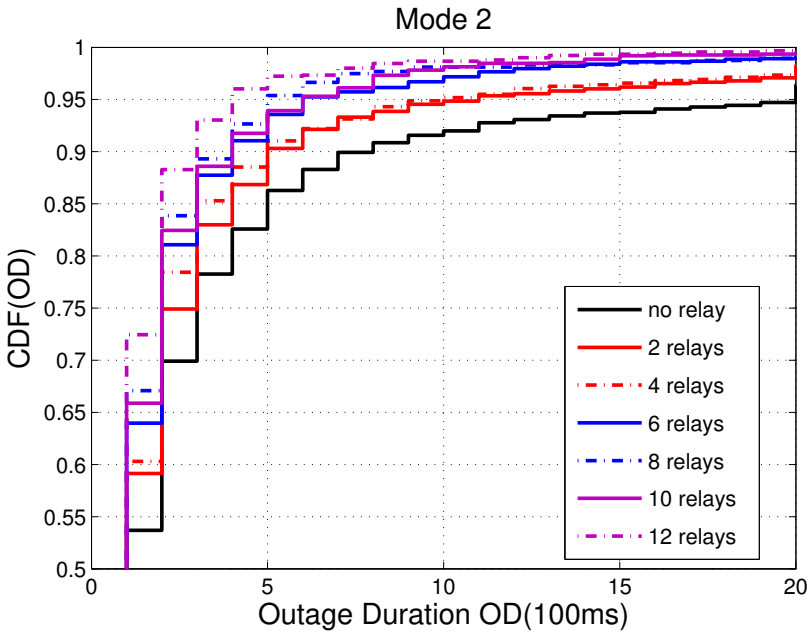

Figure 2.10: Cumulative Distribution Function of Outage Duration of Mode 2 (with Rayleigh fading)

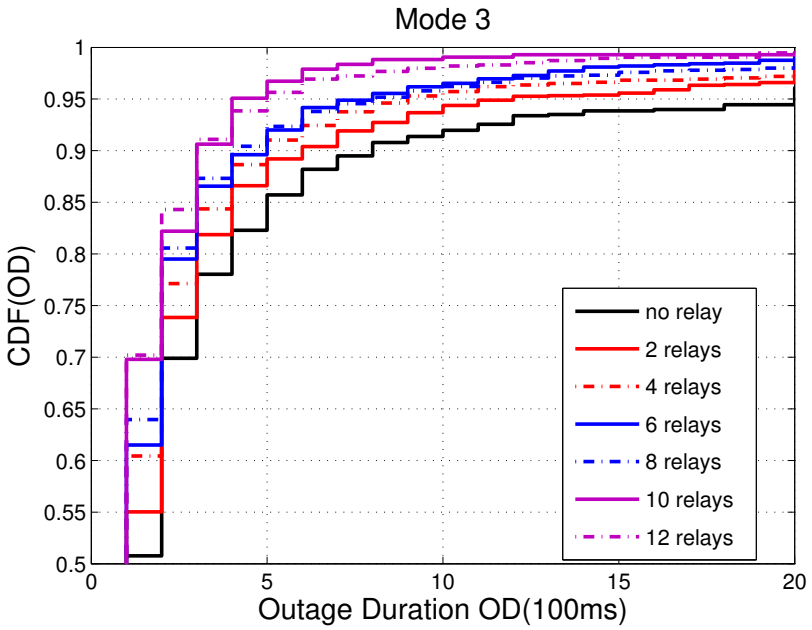

Figure 2.11: Cumulative Distribution Function of Outage Duration of Mode 3 (with Rayleigh fading)

The outage probabilities and durations are shown to indicate the potential user experience improvement when using a real-time application.

First, numerical analysis and simulation results of outage probabilities in Mode 1 is shown in Figure 2.5. The numerical analysis has high computational complexity and is difficult to apply to outage duration analysis. Therefore a simulation is necessary to study the system. Considering the computational complexity, to show that our simulation is validated by analysis, partial comparison between numerical analysis and simulation results is shown in Figure 2.5, which indicates that our simulation code is correct and can be used to study the system.

Second, we simulate the distribution of the best channel gain for the channel between the MS and BS or relays. Figure 2.6, 2.7 and 2.8 plot the distribution of the user channel gain of the three different relay deployment modes and 6 different relay densities. As shown in the figure, the intersection of the dashed arrow and the cumulative distribution function (cdf) plots indicates that as relay density increases, the percentage of outages reduces. The dashed arrow points to $122.5dB$ which is the lowest channel gain to guarantee the SNR to be above $8dB$, in which case 16-QAM with 1/2 code rate will still work. Considering the power constraints, the complexity and cost of placing relays and received SNR requirements, finding a proper relay density is very important. Beyond a certain relay density, increasing the relay density will not give significant additional performance improvement. In all modes, it is shown that relays can mitigate the shadow fading efficiently. For example, in the Mode 1 case, 10 relays can improve the performance by reducing the probability of outage by 40% compared to the no relay case. To compare the results across the three different modes, we take the 10 relay case as an example. For this case, Mode 1 has an outage probability 3% less than Mode 2 and 10% less than Mode 3. In addition, we compare the three different modes from the

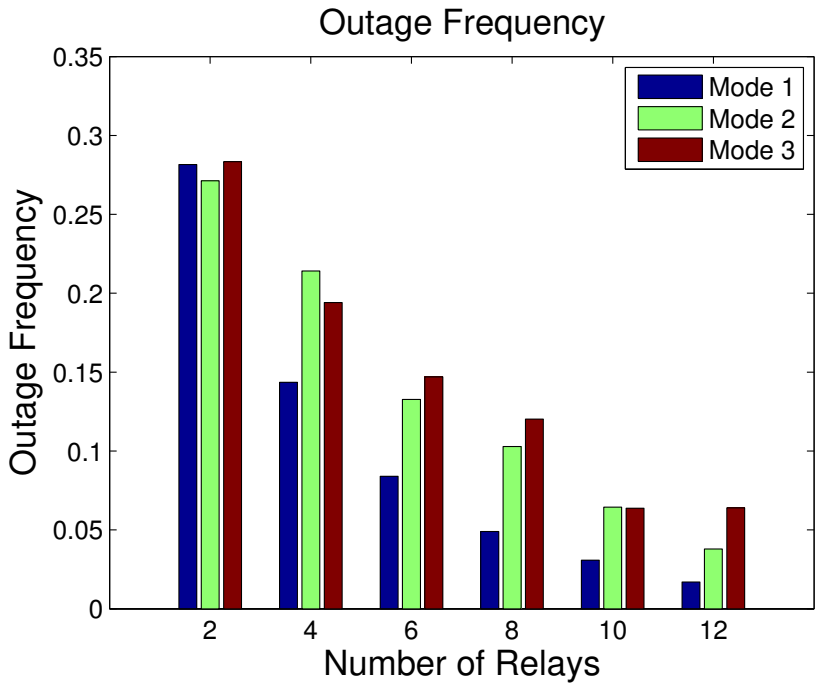

Figure 2.12: Outage Frequency of Three Modes with Different Relay Densities

outage frequency point of view. Outage frequency is defined as

$$f_{outage} = \frac{\text{Total Number of Outage Points}}{\text{Total Number of Simulation Points}}. \tag{2.25}$$

Figure 2.12 shows the result of outage frequency of the three different modes and different relay densities. From this result, we can see that Mode 1 performs better than Mode 2 and Mode 3. This is due to the randomness of the relay deployment, which works against outage prevention for this model. In some cases Mode 3 performs better than Mode 2. This occurs when most of the relays in Mode 2 are placed in deep shadow areas and are therefore ineffective.. The ideal relay deployment scheme would place relays at the edge of a deep fading area so that relays can successfully receive signals from the BS. On the average, random placement (Mode 3) is the worst choice among the three cases in our simulation.

For real-time applications, outage duration and outage frequency are both very important factors from the user experience point of view. Long outage duration and high outage frequency will lead to poor delay performance or even loss of packets. Figure 2.12 indicates that higher relay density will result in lower outage frequency. Next we investigate the outage duration experienced by the MS with different relay deployments. Outage duration performance is given in Figure 2.9, 2.10 and 2.11, which shows the cumulative distribution functions for outage durations for all three different modes. Here, we just show the distribution of outage duration from $100ms$ to $2s$ ($100ms$ is the smallest simulation time period). Under the SNR requirement given as $8dB$, it is shown that as the relay density increases, the probability of long outage duration decreases quickly. In Mode 1, with 4 relays, the probability of outage duration longer than $400ms$ is less than 10%. In Mode 2 and Mode 3, to achieve this, 6 and 8 relays are needed, respectively. For real-time video conferencing, the largest tolerable delay is around $200ms$. Our results indicate that in Mode 1 we do not need more than 6 relays to guarantee the probability of outage duration larger than $200ms$ to be less than 15%. In Mode 2 and Mode 3 more than 12 relays are needed to achieve this objective. Since we put the SNR requirement as $8dB$, which guarantees a small bit error rate (BER) of 16-QAM, the relay density needs to be high. If we reduce the SNR requirement and change the modulation, it is possible that the probability of outage duration longer than $200ms$ will become smaller or even close to 0. If there is no relay in the cell and an MS enters into a deep fading area, then due to correlated shadow fading, this outage duration will last for a long time. The longest outage duration in our simulation is $10s$ with no relay. From Figure 2.9, 2.10 and 2.11 we can observe that the probability of an outage duration greater than $2s$ is approximately 5% without relaying. Comparing the no relay case with

the 6 relays case in Mode 1, it is shown that relays efficiently reduce the lengthy outages which are caused by deep shadow fading, with the probability of outage duration greater than $2s$ reduced to less than 1%. All these results indicate that relays can mitigate the deleterious effects of correlated shadow fading efficiently.

2.6 Chapter Summary

In this chapter, we investigate the correlated shadow fading problem in a single cell cellular network and shows that it could lead to correlated outage and long outage durations. A correlated outage field is presented in this chapter. To mitigate shadow fading, relays can be deployed. The performance of three different relay deployments with different relay densities are studied. Theoretical analysis and simulations of outage performance are given to compare between different relay placement scenarios. Through these simulation, we showed that uniformly spaced relays perform better than the randomly spaced, due to the randomness of relay deployment. In following chapters, we will consider different shadow fading correlation model and extend the research to a multi-cell system.

Chapter 3

Single-Cell System Performance Analysis under Exponential Correlated Shadow Fading

Shadow fading has been proven to be a significant contributor to channel variations in wireless communication. In most cases shadow fading is assumed to have a log-normal fading distribution to model the loss at a certain location. However, in a mobile network, it is also important to know how shadow fading is correlated both in space and in time, which can greatly affect application layer behavior and service quality. This chapter is an attempt to characterize shadow fading so as to accurately study its impact on the application layer quality of service. If the correlation is strong over time and space, shadow fading can result in a long outage. In this chapter, we assume shadow fading is exponentially correlated in space. To study correlated shadow fading and its resultant outage durations, a first-order Markov chain model is developed and validated. The Markov chain model is constructed by partitioning the entire shadow fading range

into a finite number of intervals. The state transition matrix of the Markov chain is derived from the joint probability distribution of correlated log-normal shadow fading. Based on the proposed Markov chain model, the frequency and duration of outage near the edge of a single cell is analyzed. To validate the Markov chain model, correlated Gaussian random fields are simulated to analyze the outage frequency and durations due to correlated shadow fading. Comparing the simulation results with the Markov chain model results, we can conclude that the proposed Markov chain model is an efficient way to describe the channel variations, and the user experienced outage behavior of the channel.

3.1 Background

In the past few decades, fading in wireless communication systems has been studied extensively in the literature. Fading phenomena can substantially affect the performance of a wireless communication system. In general, fading can be divided into two categories: large-scale fading and small-scale fading. A signal transmitted from source to destination will experience both large-scale and small-scale fading. Small-scale fading is caused by multipath propagation. Large-scale fading, which is also known as shadow fading, is caused by obstacles (trees, buildings, etc.) in the propagation path. Shadow fading is approximated by an independent log-normal distribution [31] in most cases. Researchers have also shown that shadow fading is spatially correlated at different positions on the propagation path [14], [45]. The spatial correlation of shadow fading is important when studying the quality of service of a mobile system since it will result in long-lasting outage durations, which will deteriorate the performance of the applications running on the network. For example, in Figure 3.1, the user is moving behind a row

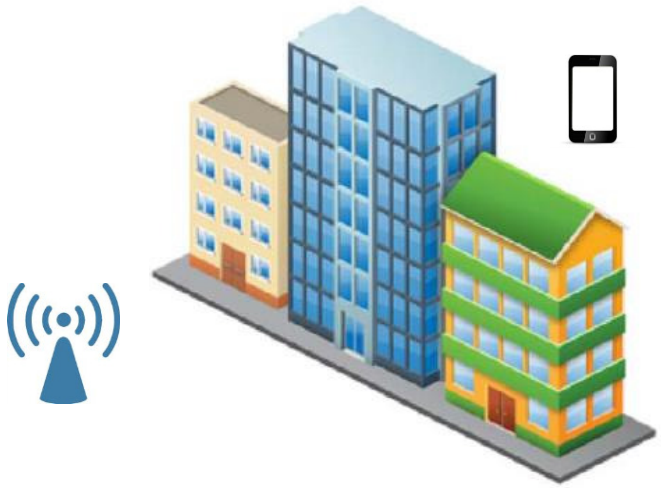

Figure 3.1: An example of building blockage

of tall buildings which block the signals from the base station. These tall buildings result in deep shadow fading, and the shadow fading of different positions behind these buildings are closely correlated.

The spatial correlation of shadow fading has been investigated by numerous researchers. Based on empirical measurements, different autocorrelation models have been proposed for different scenarios and radio frequencies [14, 46, 47]. Szyszkowicz et al. [13] studied shadow fading correlation models and investigated the feasibility of all these models. Among all these models, the analytical model proposed by Gudmundson [14] based on empirical measurements of $900MHz$ frequency is the one which is widely used in channel estimation. This model shows that shadow fading can be modeled as a first-order autoregressive process AR(1), which indicates a spatial exponential decaying autocorrelation function. Given this model, we propose a Markov chain model that can be constructed to capture the variation of shadow fading. The Markov chain models can in turn be used to accurately model the impact of shadow fading on higher layer protocols and applications. Since the shadow fading statistically follows a log-normal distribution,

we can divide the entire range of shadow fading, which is $[-\infty, +\infty]$ into a finite number of intervals. Each interval is considered as a state of the Markov chain model. When the shadow fading falls in a particular interval, it is assigned to be in this particular state. The number of intervals (states) defines the granularity of the Markov chain model. The higher the number of states, the higher the precision in modeling the shadow fading. Correlated log-normal shadow fading has different variances with regard to different scenarios. For example, urban and suburban areas have different standard deviations based on empirical measurements. Different standard deviations of the log-normal shadow fading will result in different state transition matrices of the Markov chain model.

Outage events happen when the channel state is poor, and the received signals are not strong enough for the receiver to decode. Outage probability and the length of outage duration are important performance measurements of a wireless communication system over fading channels. Considering the applications which require low latency where buffer size is small, a long outage duration will drop the connection and lower the quality of service. To study the outage behavior of a communication system under correlated shadow fading, a well designed Markov chain model is a powerful tool. With a Markov chain model, the channel state in the next user position can be estimated from the current channel state given the current user position. Therefore, the system performance can be evaluated efficiently. Fading is a significant factor which causes dramatic channel state variations. Correlated shadow fading will result in long-lasting outage durations which is harmful to delay-sensitive real-time application and result in loss of quality of service. The Markov chain model can be used to analyze the probability distribution of outage events. The distribution and behavior of outage events will provide us the necessary information to improve wireless communication systems further.

For example, efficient cooperative communication schemes can be designed to mitigate the outage behavior.

The main focus of this chapter is how to design a first-order Markov chain model to reflect the spatial correlation of shadow fading, and the study of outage behavior of a single cell wireless communication system given correlated shadow fading. The key contributions of this chapter are summarized below.

- Constructed a Markov chain model based on correlated shadow fading.
- Analyzed the outage frequency and outage duration of a single cell wireless communication system over correlated shadow fading.

The remaining sections of this chapter are organized as follows. The channel model with spatial correlated shadow fading is described in Section 3.2. Section 3.3 shows how to construct the Markov chain model from the correlated shadow fading. Analysis of outage behavior is demonstrated in Section 3.4. Simulation to validate the Markov chain model is illustrated in Section 3.5. Section 3.6 summarizes and concludes the chapter.

3.2 Channel Model with Correlated Shadow Fading

To simplify the problem, we consider a single 4G LTE cell without any intercell interference in Figure 3.2(b). Due to the high bandwidth of OFDM systems, LTE networks are more resilient to frequency selective fading [31], therefore in this chapter small-scale fading is ignored and shadow fading becomes the most important fading factor. There is a Base Station(BS) at the center of the cell.

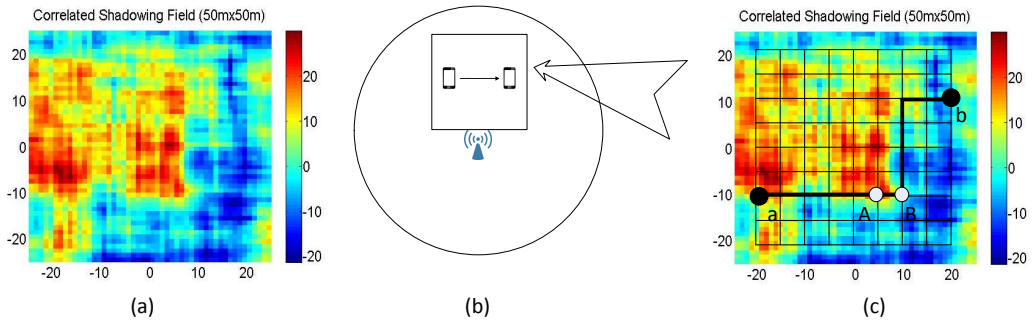

Figure 3.2: (a) A typical exponential correlated shadow fading field in a $50m \times 50m$ area. The color bar denotes the value of the shadow fading in dB. (b) A single cell model with a MS moving on a fixed trajectory. (c) A locally generated correlated shadowing field for a fixed trajectory from point a to point b.

A Mobile Station (MS) is moving on a certain trajectory within the cell. The received signal on a link $(S \rightarrow D)$ between source and destination is given by:

$$y_D = G_{SD} x_S + n_D, \tag{3.1}$$

where x_S is the signal transmitted by the source and y_D is the signal received by the destination. $n_D \sim \mathcal{CN}(0, N_0)$ is additive white Gaussian noise. G_{SD} is the channel gain from source to destination including path loss and shadow fading. SNR $\triangleq P*G_{SD}^2/N_0$, is the end-to-end received signal-to-noise ratio (SNR). The destination successfully receives the signals if no outage event happens, i.e., $\log_2(1+\text{SNR}) \geq R$, where R is the required data rate. From the definition of SNR, no outage event happens as long as $G_{SD}^2 > \beta$, where $\beta = \frac{(2^R-1)*N_0}{P}$. Therefore the channel gain from transmitter to receiver determines if an outage will occur.

Here we rewrite the channel gain in the following form: $G_{dB} = PL(d) + S$, where G_{dB} is G_{SD} in dB, PL denotes the propagation pathloss in dB, d is the distance from BS to MS and S denotes shadow fading factor. In most cases, shadow fading is modeled as an independent log-normal distribution [20] with a standard deviation derived from empirical measurements. In this model, the

probability distribution of pathloss G_{dB} is given by:

$$p(G_{dB}) = \frac{1}{\sqrt{2\pi}\sigma_{G_{dB}}} exp[-\frac{(G_{dB} - \mu_{G_{dB})^2}}{2\sigma^2_{G_{dB}}}], \tag{3.2}$$

where $\mu_{G_{dB}}$ is the average pathloss which is equal to $PL(d)$ and $\sigma_{G_{dB}}$ denotes the standard deviation of pathloss. Since shadow fading is the only fading factor that is considered here, $\sigma_{G_{dB}}$ is determined by the standard deviation of shadow fading. This model fails to capture the spatial correlations in shadow fading. For examples, in Figure 3.2(c), shadow fading factors of two close positions A and B, which are S_A and S_B, are not independent but correlated to each other. Empirical measurements showed that shadowing has significant correlations in several realistic scenarios and the correlated shadow fading can affect system performance [21]. Among all models derived from empirical measurements for correlated shadow fading, exponentially decaying correlation [14] is widely used. In this chapter, we choose this model to do further analysis. Figure 3.2(a) is an example of exponentially correlated shadowing field which is generated from the Graziano model [21]. This figure shows a $50 \times 50m^2$ shadow fading area and illustrates that deep shadowing area is clustered and correlated (the blue area).

In Figure 3.2(c), the entire space is discretized. The MS moves on the lattice as shown. A and B are two neighbouring points. Assume the shadow fading (in dB) is $N(0, \sigma^2)$ where σ is the standard deviation, the spatial correlation between S_A and S_B will be given by

$$\rho_{A,B} = \frac{E[S_A S_B]}{\sigma^2} = e^{-\frac{d_{A,B}}{d_0}}, \tag{3.3}$$

where $d_{A,B}$ is the distance between A and B, d_0 denotes the de-correlation distance

[48], which means if the distance between two points are substantially greater than d_0, the two shadow fading will be independent to each other. d_0 is determined by the environment, therefore urban and suburban areas have different de-correlation distances. An exponential correlation implies the shadow fading samples can be written as an AR(1) process as follows [49]:

$$S_B = \rho S_A + (1 - \rho) n_A, \tag{3.4}$$

where n_A denotes the channel noise at A. From this we conclude that the next channel state can be determined from the current channel state and the distance MS moves.

3.3 Markov Chain Model

In this section, we will construct a Markov chain model for exponential correlated shadow fading. First of all, we will discretize the space. In Figure 3.2(c), the space was partitioned into unit square spaces of $5 \times 5m^2$ (This granularity is used to describe the Markov chain model while in the simulation we uses a finer granularity). The MS moves on the lattices from point to point, the distance between each two neighboring points are considered as a unit distance δd. We prove that shadow fading factors of any two points that can be connected by a trajectory having jointly Gaussian distribution.

Lemma 1. Exponential correlated shadow fading factors of any two points that can be connected by a trajectory have a jointly Gaussian distribution.

Proof. Suppose the two points are a and b, since there exists a trajectory connecting a and b like in Figure 3.2(c), we can assume there are n positions on this

trajectory $(t_1, t_2, \ldots, t_n)$. Then follow equation (3.4), we have the following:

$$\begin{aligned} S_b &= \rho S_{t_n} + (1-\rho) n_{t_n} \\ &= \rho(\rho S_{t_{n-1}} + (1-\rho) n_{t_{n-1}}) + (1-\rho) n_{t_n} \\ &= \ldots\ldots \\ &= \rho^n S_{t_1} + \sum_{i=1}^{n} \rho^{n-i}(1-\rho) n_{t_i} \\ &= \rho^{n+1} S_a + \rho(1-\rho) n_a + \sum_{i=1}^{n} \rho^{n-i}(1-\rho) n_{t_i}. \end{aligned} \tag{3.5}$$

Let $X = \alpha S_a + \beta S_b$, from equation 3.5, the following can be derived:

$$X = \alpha S_a + \beta(\rho^{n+1} S_a + \rho(1-\rho) n_a + \sum_{i=1}^{n} \rho^{n-i}(1-\rho) n_{t_i}). \tag{3.6}$$

Since S_a, n_{t_i} and n_a are all independent and Gaussian random variables, we conclude that X is also Gaussian, which implies that S_a and S_b are jointly Gaussian. □

Given the above conclusion, a Markov chain model can be constructed as follows:

- Divide the entire shadow fading range $[-\infty, +\infty]$ into a finite number of intervals $\{[-\infty, S_0], [S_0, S_1], \ldots, [S_N, +\infty]\}$. Each interval represents a state of the Markov chain model.
- Derive the state transition matrix of the Markov chain model from the probability distribution of the correlated shadow fading.
- Derive the steady-state probability from the state transition matrix of the Markov chain model.

To derive the state transition matrix of the Markov chain model, we first investigate the probability density function of the correlated shadow fading. Since we have discretized the entire space into unit distances, here the state transition probability from point A to point B will be defined and used to calculate the state transition matrix of the Markov chain. Since S_A and S_B are jointly Gaussian with a correlated coefficient ρ_0, according to [50], we have

$$\begin{aligned} f_{S_A|S_B=s_B}(s_A) &= \frac{f_{S_A,S_B}(s_A,s_B)}{f_{S_B}(s_B)} \\ &= \frac{1}{\sigma_A\sqrt{2\pi(1-\rho_0^2)}}\exp\{-\frac{(s_A-(\mu_A+\sigma_A\rho_0(s_B-\mu_B)/\sigma_B))}{2\sigma_A^2(1-\rho_0^2)}\}, \end{aligned} \tag{3.7}$$

where μ_A and μ_B are expectations of log-normal shadow fading S_A and S_B, which is typically set to 0, while σ_A and σ_B are standard deviations, which are assumed to be equal to σ_0. Based on these assumptions, we can rewrite the equation as follows:

$$f_{S_A|S_B=s_B}(s_A) = \frac{1}{\sigma_0\sqrt{2\pi(1-\rho_0^2)}}\exp\{-\frac{s_A-\rho_0 s_B}{2\sigma_0^2(1-\rho_0^2)}\}. \tag{3.8}$$

Assume there are N states of the Markov chain model $ST_1, ST_2, \cdots, ST_N$ where ST_i corresponds to the interval $(S_{i-1}, S_i]$. Then we have the state transition probability as follows:

$$\begin{aligned} P_{i,j} &= P(S_A \in ST_j | S_B \in ST_i) \\ &= \frac{P(S_A \in ST_j, S_B \in ST_i)}{P(S_B \in ST_i)} \\ &= \frac{\int_{S_{i-1}}^{S_i}(\int_{S_{j-1}}^{S_j} f_{(S_A|S_B=s_B}(s_A)ds_A)f(s_B)ds_B}{\int_{S_{i-1}}^{S_i} f(s_B)ds_B}. \end{aligned} \tag{3.9}$$

From equation (3.9), the state transition matrix of the Markov chain can be derived. The steady-state transition matrix can be determined by P.

3.4 Analysis of Outage Behavior

In this section we analyze the outage behavior of the communication system using the Markov chain model of correlated shadow fading. The outage duration of a system is a significant factor influencing system performance. Given a fixed mobile trajectory, the Markov chain model described in Section 3.3 provides an efficient way to study the outage events. In Figure 3.2(c), a fixed trajectory is given from point a to b through several intermediate points. Considering two consecutive points A and B, we have $G_A = PL_A(d_A)+S_A$ and $G_B = PL_B(d_B)+S_B$ in dB. The probability that A and B are both in an outage area can be written as:

$$\begin{aligned} &P(G_A < \gamma, G_B < \gamma) \\ &= P(S_A < \gamma - PL_A(d_A), S_B < \gamma - PL_B(d_B)). \end{aligned} \tag{3.10}$$

If $S_A < \gamma - PL_A(d_A) \in ST_i$ and $S_B < \gamma - PL_B(d_B) \in ST_j$, we can infer that, to avoid outage, the lower bound of the shadow fading factor S_A is in state ST_i and for S_B is in state ST_j. State ST_i and ST_j are called lower bound states. Based on this approximation, the above probability can be written as:

$$P(G_A < \gamma, G_B < \gamma) = \sum_{m=0}^{i} \sum_{n=0}^{j} P(ST_m) \bullet P(ST_m, ST_n) \tag{3.11}$$

where $P(ST_m)$ is the probability that S_A is in the range of ST_m which can be calculated from the Gaussian distribution. $P(ST_m, ST_n)$ can be found from the state transition matrix. Following this, the probability of an outage duration of

$$P = \begin{bmatrix} P1 \\ P2 \\ P3 \\ P4 \\ P5 \\ P6 \\ P7 \\ P8 \end{bmatrix} \tag{3.13}$$

length $l > L$ can be derived in below:

$$\begin{aligned} &P(G_1 < \gamma, \ldots, G_L < \gamma) = \\ &\sum_{m_1=0}^{M_1} \cdots \sum_{m_L=0}^{M_L} P(ST_{m_1}) \bullet P(ST_{m_1}, ST_{m_2}) \\ &\bullet \ldots \bullet P(ST_{m_{L-1}}, ST_{m_L}), \end{aligned} \tag{3.12}$$

where M_i, $i \in \{1, \ldots, L\}$ are corresponding lower bound states of each position on the trajectory.

$$
\begin{aligned}
P1 &= \begin{bmatrix} 0.5580 & 0.3627 & 0.0757 & 0.0036 & 3.5243\times10^{-5} & 0 & 0 & 0 \end{bmatrix} \\
P2 &= \begin{bmatrix} 0.1587 & 0.4404 & 0.3359 & 0.0624 & 0.0026 & 2.3466\times10^{-5} & 0 & 0 \end{bmatrix} \\
P3 &= \begin{bmatrix} 0.0184 & 0.1788 & 0.4546 & 0.2980 & 0.0484 & 0.0018 & 1.4485\times10^{-5} & 0 \end{bmatrix} \\
P4 &= \begin{bmatrix} 0.0007 & 0.0258 & 0.2165 & 0.4624 & 0.2573 & 0.0361 & 0.0012 & 8.4341\times10^{-6} \end{bmatrix} \\
P5 &= \begin{bmatrix} 8.4341\times10^{-6} & 0.0012 & 0.0361 & 0.2573 & 0.4624 & 0.2165 & 0.0258 & 0.0007 \end{bmatrix} \\
P6 &= \begin{bmatrix} 0 & 1.4485\times10^{-5} & 0.0018 & 0.0484 & 0.2980 & 0.4546 & 0.1788 & 0.0184 \end{bmatrix} \\
P7 &= \begin{bmatrix} 0 & 0 & 2.3466\times10^{-5} & 0.0026 & 0.0623 & 0.3359 & 0.4404 & 0.1587 \end{bmatrix} \\
P8 &= \begin{bmatrix} 0 & 0 & 0 & 3.5243\times10^{-5} & 0.0036 & 0.0757 & 0.3627 & 0.5580 \end{bmatrix}
\end{aligned}
\tag{3.14}
$$

In this section, we employ Monte-Carlo simulation to validate our Markov chain model. To start the simulation, a large number of correlated shadowing fields are generated. As shown in Figure 3.2(b) and (c), instead of generating shadowing fields for the entire cell, we pick up a MS trajectory and generated shadowing fields that covers that trajectory. In this chapter, we choose the urban environment as the case to study. In this case, the shadow fading and Markov chain parameters are set as in Table 3.1. The standard deviation of shadow fading is chosen to be $8dB$ following [13]. The number of states of the Markov chain is set to be $3 * \sigma_0/n * 2 + 2$, where $n = 1, 3, 8$ is the size of each range (state) in dB except the two above $3\sigma_0$. n in this case represents different granularities in the area of $[-3\sigma_0, 3\sigma_0]$. The state transition matrices are calculated with regard to

Table 3.1: Simulation Configuration Parameters

Okumura-Hata Model	BS Height: $100m$ MS Height: $1m$
	De-Correlation Distance d_0: $20m$ Standard Deviation σ_0: $8dB$
Correlated Shadow Fading Markov Chain Model	Number of States: 50, 18, 8 $(3 * \sigma_0/n * 2 + 2,\ n = 1, 3, 8)$
MS Trajectory	Unit Distance δd: $1m$
Shadowing Field	$50 \times 50m^2$
Radio Frequency	$f : 1024MHz$
BS Transmission Power	$P : 30dbm$
SNR Requirement	$10dB$

each n. For example, when $n = 8$, the states of the Markov chain model are

$$\begin{aligned}&[(-\infty, -24], (-24, -16], (-16, -8], (-8, 0],\\ &[0, 8], [8, 16), [16, 24), [24, +\infty)],\end{aligned} \tag{3.15}$$

and the state transition matrix is given in (3.13 and 3.14).

3.5 Simulation Results

To validate our Markov chain models, the probability distributions of outage durations corresponding to MS trajectories of length $l > 1m$ up to $l > 9m$ are studied given different number of states. Since there is a trade-off between the number of states and the complexity of the simulation computation, the simulated results also provide us information about the proper granularity of the Markov chain model to most accurately approximate the real channel. The simulation also confirms that correlated shadow fading indeed can cause long-lasting outage durations. In our simulation, the MS moves on a straight track which is around

$900m$ away from the BS. Let l denote the outage duration in meters, Figure 3.3 shows the probability of $l > L$. Comparing the two cases: with and without correlation, we can conclude that correlated shadow fading can result in severe long-lasting outage durations. Take $L = 5$ for example, the correlated case gives $P(l > L) = 12\%$, while in the non-correlated case the probability is around 0%. This illustrates the correlation between shadow fading cannot be neglected in mobility models. The MS speed is approximately the same as pedestrian speed which is $1m/s$ (Since the edge length of the lattice is $1m$, the MS moves one grid (unit distance) every second). Assuming this, the user will experience an outage of more than 9 seconds with a probability of 7%.

To find out the proper number of states of the Markov chain model, three different Markov chain models with different number of states are tested. Basically we divide the $[-3\sigma_0, 3\sigma_0]$ area with different granularity, which is represented by $n = 1, 3, 8$. When $n = 1$, the interval ST_i except $(-\infty, S_0]$ and $[S_N, +\infty)$ is $1dB$. The results showed in Figure 3.3 indicates that when $n = 1$, the curve is close to the correlation curve, which means that the Markov chain model becomes a good approximation of the channel to study the outage behavior of the system. Generally, more Markov states lead to more precise models. When the interval $[S_i, S_j]$ becomes relatively large with regarding σ_0, the Markov chain model will fail to be a useful tool to study the outage behavior of the system. For example, in Figure 3.3, when $n = 8$, $P(l > 1)$ is almost twice the correct $P(l > 1)$. The prediction of the outage behavior of the system is not precise and useful anymore.

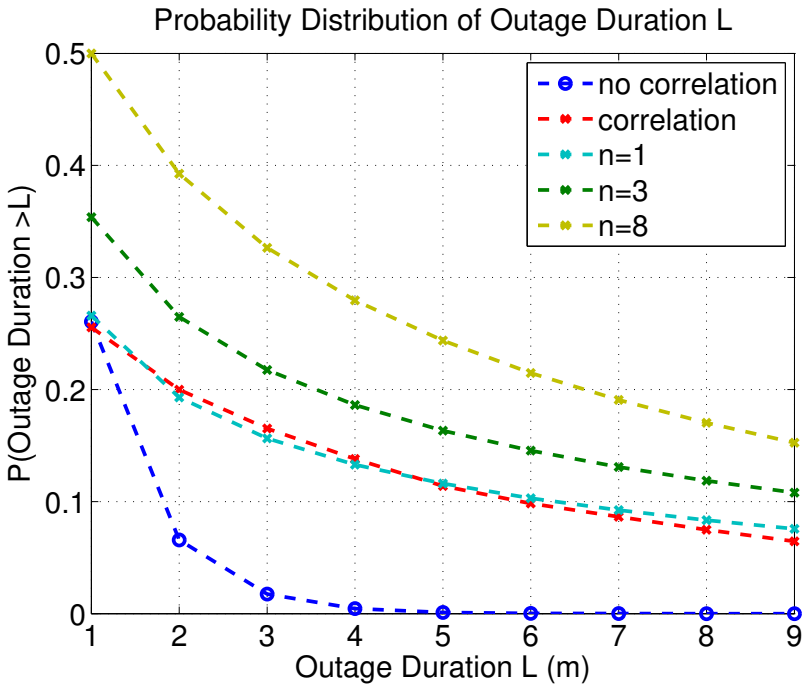

Figure 3.3: Probabilities of outage duration greater than L

3.6 Chapter Summary

In this chapter we investigated how shadow fading at different positions in a cellular network is correlated. In an environment where the correlation is high, shadow fading will result in long-lasting outage durations which can lead to a significant deterioration in system performance. To model spatially correlated shadow fading we divided the entire range of shadow fading into a finite number of intervals. A Markov chain model is then constructed, where each interval becomes a state of the Markov chain model. This model can be used to analyze the outage behavior at the application layer. We demonstrated that a well designed Markov chain model with an appropriate number of states corresponding to the standard deviation of the shadow fading is indeed a powerful tool to study system performance. For a single-cell system, this Markov chain model is able to analyze the system performance because there only exist autocorrelation in this scenario.

In next chapter, we will investigate the system performance of a multi-cell system. This Markov chain model will not be capable to describe the scenario there. Instead, we will run numerical simulations to show the system performance of a multi-cell system under exponentially correlated shadow fading.

Chapter 4

Multi-Cell System Performance under Exponential Correlated Shadow Fading

In a multi-cell cellular network, connections between the Base Station (BS) and Mobile Stations (MSs) may fail when the channel has low signal-to-interference-plus-noise ratio (SINR). Shadow fading is a large-scale fading, which can cause significant received power loss and reduce SINR for a wide area. Correlated shadow fading will result in correlated long-lasting outage durations in a multi-cell system. Increasing the BS density to make the network denser is a common way to increase SINR, reduce the number of long-lasting outage durations and provide better Quality of Service (QoS) support for delay sensitive applications. In Chapter 2 and Chapter 3, we discussed mitigating shadow fading in a single-cell model. This chapter extends the work in Chapter 3 and focuses on the study of the performance of a multi-cell communication system under correlated shadow fading. We consider the downlink direction in a multi-cell communication system.

The outage probability of two system layouts, Grid model and Random model, are presented given correlated shadow fading and different BS densities. First, we compare the outage probability of the two different BS layout models with the same correlated shadow fading. Simulation results indicate that the Grid model has better performance than the Random model. Secondly, the outage probability with independent shadow fading or correlated shadow fading for the Random model is demonstrated. SINR is calculated under the assumption of the existing independent shadow fading and correlated shadow fading. Thirdly, we focus on the Random model, which is more realistic, and present the distribution of outage durations given independent shadow fading or correlated shadow fading. Simulation results demonstrate that outage durations with correlated shadow fading are longer than those with the independent shadow fading. At the end, we show that increasing the BS density can mitigate the effect of correlated shadow fading and improve the system performance by reducing the outage probability and shortening outage durations.

4.1 Background

There have been a lot of studies on the outage probability of cellular communication systems [51–53]. The author of [54] analyzed the outage probability and coverage area under independent and identically distributed ($i.i.d$) shadow fading which follows Log-normal distribution, Weibull distribution and Gamma distribution. In contrast, there is much less work on the outage probability and outage duration, given the correlated shadow fading. The performance of a multi-cell system given correlated shadow fading remains to be an open problem. In [55] and [56], we discussed the outage probability and the outage duration distribu-

tion of a single-cell communication system under the exponentially correlated shadow fading and the distance-angle correlated shadow fading. For a single-cell model, exponentially correlated shadow fading can be modeled as a Markov chain model. Highly correlated shadow fading will result in long-lasting outage durations. In [56], a single-cell model under the distance-angle correlated shadow fading is investigated. The correlated shadow fading leads to correlated outage events and long-lasting outage durations. To overcome these disadvantages, we propose a cooperative communication scheme to mitigate shadow fading by deploying relays at the cell edge. Chapter 2 and Chapter 3 are limited to the single-cell model. In this chapter, we are going to extend the study to review the impact of correlated shadow fading on a multi-cell model, and provide a solution to overcome the long-lasting outage durations.

For the multi-cell system, a new general model for the user SINR was developed using stochastic geometry [57]. The cellular network was modeled by placing BSs at locations as a homogeneous Poisson Point Process (PPP). The author concluded that, under general fading, increasing the number of BS did not affect the coverage probability and/or the outage probability, as long as the MS was connecting to the nearest BS. Moreover, the paper did a comparison between the grid model and the PPP model, and concluded that the regular grid model provided the upper bound of the coverage probability while the PPP model provided the lower bound. The author also considered the effect of independent log-normal interference and concluded that the increasing log-normal interference increased the coverage probability, which is counter-intuitive. However, in this paper, the author did not consider the scenario with correlated log-normal shadow fading. Nevertheless, only the coverage probability was characterized, whereas outage duration has not yet been analyzed.

A comparative analysis of the random topology and the grid topology of a small cell network deployment was given in [58]. In this paper, the spatial outage probability and the spatial average throughput, versus the number of access points of the two different network deployments were illustrated under independent shadow fading. Approximate the outage probability and the capacity for $\kappa - \mu$ shadow fading was discussed in [59]. $\kappa - \mu$ shadow fading includes one-side Gaussian, the Rayleigh, the Nakagami-m and the Rician. As we mentioned before, the empirical measurements didn't exhibit such complicated features of shadow fading. Therefore, those complex features are not the main focus when investigating system performance under correlated shadow fading.

The key contributions of this chapter are summarized as follows:

- Correlated outage fields are given to analyze the relationship between correlated shadow fading and correlated outage events.
- Investigate outage probability of both the Grid model and the Random model given correlated shadow fading.
- Illustrate how increasing the BS density helps mitigate the correlated shadow fading for the Random model in terms of reducing the outage probability (coverage probability) and the percentage of long-lasting outage durations.
- Analyze the relation between the tunable parameter (de-correlation distance) of the correlated shadow fading model and the outage probability.
- Compare the performance of the system with regard to different MS-BS connection strategies: MS connecting to the nearest BS versus MS connecting to the BS providing strongest signal.

The chapter is organized as follows: Section 4.2 presents the correlated shadow fading model used in this chapter and the resultant correlated outage field. Section 4.3 illustrates the system model with two different BS deployments and investigates the outage probability given the two deployments. Section 4.4 gives a theoretical analysis of the outage probability given correlated shadow fading. Section 4.5 presents the simulation setup and analyzes the simulation results from different BS densities. Section 4.6 summarizes the chapter and proposes future work directions.

4.2 Correlated Shadow Fading

As stated in Chapter 2, empirical measurement shows that there exists different patterns of correlations between shadow fading at different positions. The independent log-normal shadow fading model, while is very useful for static MS performance analysis, cannot reflect the spatial correlation of shadow fading between different locations. In this section, we will give a brief introduction of shadow fading models, including the model which will be utilized in this chapter. In Chapter 2, a distance-angle correlation model is used. In Chapter 3 an exponential correlation model is used. The correlation matrix of the distance-angle model is given below:

$$\mathbf{K}_{N\times N} = [\sigma_s(\vec{r_i})\sigma_s(\vec{r_j})h(\vec{r_i}\vec{r_j})], \tag{4.1}$$

where N paths interfere with path $\vec{r_i}$ and $\mathbf{E}\{S_i^2|\vec{r_i}\} = \sigma_s^2(\vec{r_i})$. This model assumes that in the correlation matrix, h is separable with respect to the angle of arrival

$$\theta = |\angle\vec{r_i} - \angle\vec{r_j}| \in [0^\circ, 180^\circ], \tag{4.2}$$

and the arrival distance ratio

$$R = |10\log_{10} r_i/r_j| = \frac{10}{\ln 10}|\ln r_i - \ln r_j|, \tag{4.3}$$

$$h(\vec{r_i}, \vec{r_j}) = max\{1 - \theta/\theta_0, 0\} \cdot max\{1 - R/R_0, 0\}. \tag{4.4}$$

The correlation coefficient is a piece-wise linear function (4.4) of the angle of arrival and the arrival distance ratio. This correlation model is suitable for a single-cell model when only one BS is located at the center of the cell. However, for the multi-cell model, there are quite a number of BSs at different places; both autocorrelation and cross-correlation need to be taken care of. It is not possible to choose a single BS as the center of the shadowing field. To incorporate both autocorrelation and cross-correlation, the simulation complexity will increase in dramatic order. Due to this feature, the distance-angle model is not chosen to analyze the performance of the mulit-cell system. In this chapter, the exponential correlation model is used. An exponentially correlated shadowing field S with shadow fading factor s_i for each position p_i has a correlation matrix as below:

$$\mathbf{K}_{N\times N} = [\sigma_s(p_i)\sigma_s(p_j)\rho(i,j)], \tag{4.5}$$

where N is the length of the shadowing field. Suppose A and B are two neighboring points, the shadow fading (in dB) is $N(0, \sigma^2)$ where σ is the standard deviation.

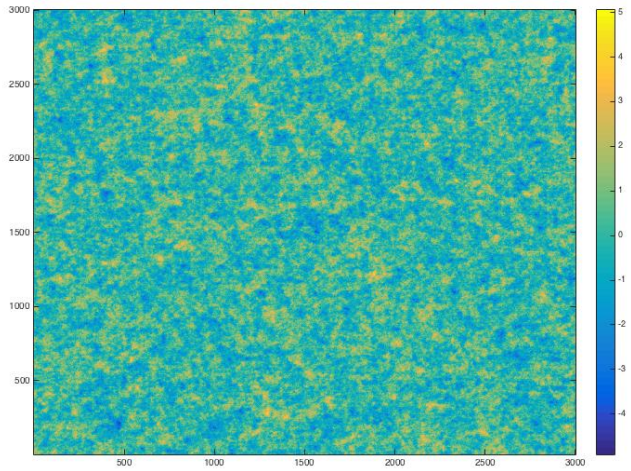

Figure 4.1: Exponentially correlated shadowing field with $d_0 = 20m$ (the color of the area refers to the normalized standard deviation, which is $S_i/\sigma_s(i)$)

The spatial correlation between s_A and s_B is given by

$$\rho_{A,B} = \frac{E[s_A s_B]}{\sigma^2} = e^{-\frac{d_{A,B}}{d_0}} \tag{4.6}$$

Following the shadowing field generation algorithm, we generate shadowing fields with different values of de-correlation distances. A sample shadowing field is shown in Figure 4.1 with 20 meters de-correlation distance.

Given a correlated shadowing field, the outage events at different locations are correlated. Without considering other small-scale fadings, the channel gain at different locations has a spatial correlation. An outage event occurs when SINR becomes less than γ, where γ is a given SINR threshold. Based on the aforementioned correlated shadow fading model and the Random model, a correlated outage field can be generated as in Figure 4.2. On the left, an outage field with independent log-normal shadow fading is shown, while the correlated outage field

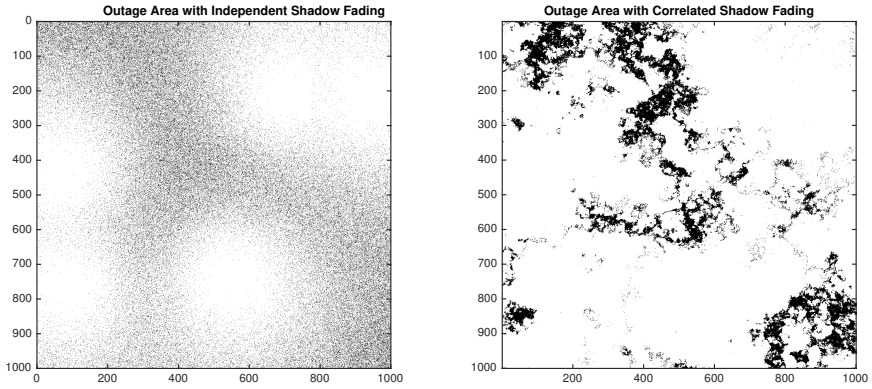

Figure 4.2: Correlated outage fields (Dark areas are outage areas while white areas are non-outage areas)

with correlated shadow fading is given on the right. The black color indicates outage areas. Outage areas due to the independent shadow fading are nonconsecutive dots. In contrast, those under the correlated shadow fading contain several connected areas . Therefore, we conclude that correlated shadow fading results in correlated outage areas with regard to the multi-cell system.

4.3 System Model

In this section, we consider two system models with two different BS deployments: the Grid model and the Random model.

- Grid model: λ BSs are placed on a regular grid deterministically.
- Random model: λ BSs are placed randomly in a fixed area.

The left subfigure of Figure 4.3 is an example of the grid model, where cells are in regular square shape with the same size. For the Random model shown in the right subfigure, cells are not guaranteed to be the same shape or the same size. Nearest distances between different cells have a large variation.

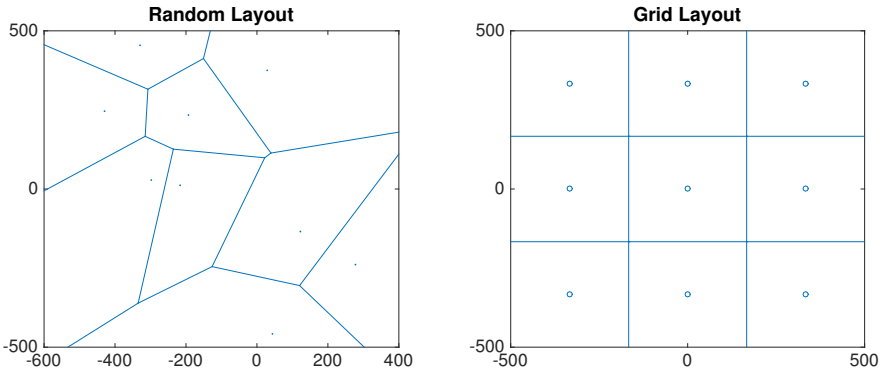

Figure 4.3: Random model and Grid model with $\lambda = 9$.

4.4 Outage Probability Analysis

Let $\varphi = \{1, 2, \ldots, N\}$ denotes the set of all BSs, then the received signal from BS i to the destination user D is given by:

$$y_{i \to D} = G_{i \to D} x_i + n_D. \tag{4.7}$$

where x_i is the signal transmitted by the source BS and $y_{i \to D}$ is the signal received by the destination user. $n_D \sim \mathcal{CN}(0, N_0)$ is additive white Gaussian noise. $G_{i \to D}$ is the channel gain from source BS to MS including path loss and shadow fading. The end-to-end received SINR is given in below:

$$\text{SINR} \triangleq \frac{P_i * G_{i \to D}^2}{N_0 + \sum_{j \in \varphi / i} P_j * G_{j \to D}^2}, \tag{4.8}$$

where P_i is the transmitted power of BS i. The MS successfully receives the signal if no outage event occurs, i.e., $\log_2(1 + \text{SINR}) \geq R$, where R is the required data rate. From the definition of SINR, no outage event occurs as long as SINR $> \gamma$, where $\gamma = 2^R - 1$.

For a particular MS, outage event occurs when its received SINR is less than a

threshold to decode the received signal. In our scenario, the probability that the receiver cannot decode signals received from its serving BS is defined as:

$$P(out_i) = P[\text{SINR}_{i\to D} < \gamma]. \tag{4.9}$$

We investigate two connection strategies:

- Nearest BS: MS chooses to connect to the nearest BS.
- Strongest BS: MS chooses to connect to the BS providing highest SINR.

In the Nearest BS mode, we assume that the MS is served by the nearest BS, then the outage probability will be

$$P_{out} = P_{out_i}, \tag{4.10}$$

where i is the index of the nearest BS.

In the Strongest BS mode, under the assumption that an MS is always connecting to the BS which provides the highest SINR, the outage event occurs if no BS can provide high enough SINR to the receiver. Based on this assumption we have:

$$P_{out} = \max_{i=1,\cdots,N} P[\text{SINR}_{i\to D} < \gamma]. \tag{4.11}$$

The probability density function (pdf) of shadow fading S given L correlated fading branches is

$$\begin{aligned} f_{\mathbf{S}}(\mathbf{s}) =& \frac{\lambda^L}{\sqrt{2\pi}|\mathbf{K}_{L\times L}|^{1/2}\prod_{i=1}^{L} s_i} \\ & \cdot \exp(-\frac{1}{2}(10\log_{10}\mathbf{s} - \boldsymbol{\mu})^T \mathbf{K}_{L\times L}^{-1}(10\log_{10}\mathbf{s} - \boldsymbol{\mu})), \end{aligned} \tag{4.12}$$

where $\lambda = 10/\ln 10$ and $\boldsymbol{\mu}$ is the average shadow fading which is normally 0. $\mathbf{K}_{L\times L}$ is the correlation matrix which is defined in (4.5). Let $\theta_i = \frac{10\log_{10} s_i - \mu_i}{\sqrt{2}\sigma_i}$, and doing a change of variables gives us the pdf of $\boldsymbol{\Theta}$ as follows:

$$f_{\boldsymbol{\Theta}}(\boldsymbol{\theta}) = \frac{1}{\pi^{L/2}|\boldsymbol{\Sigma}|^{1/2}} \exp(-\boldsymbol{\Theta}^T \boldsymbol{\Sigma}^{-1} \boldsymbol{\Theta}), \tag{4.13}$$

where $\boldsymbol{\Sigma}$ is the correlation coefficient matrix which is

$$\begin{bmatrix} 1 & h_{1,2} & \cdots & h_{1,L} \\ \vdots & \ddots & \ddots & \vdots \\ h_{L,1} & h_{L,2} & \cdots & 1 \end{bmatrix}. \tag{4.14}$$

Since $\text{SINR}_{i\to D} = PL_{i\to D} + S_i - N_0 - \sum_{j\in\varphi/i}(PL_{j\to D} + S_j)$ in dB, $\text{SINR}_{i\to D} < \gamma$ means

$$S_i - \sum_{j\in\varphi/i} S_j < \gamma - PL_{i\to D} + \sum_{j\in\varphi/i} PL_{j\to D} + N_0, \tag{4.15}$$

where φ denotes the set of all BSs. Then the outage probability can be written as:

$$P_{out} = \underbrace{\int_{-\infty}^{+\infty} \cdots \int_{-\infty}^{+\infty}}_{i=1,\cdots,N} g(PL_i S_i - \gamma \sum_{j\in\varphi/i} PL_j S_j) f(\mathbf{s}) d\mathbf{s}, \tag{4.16}$$

where $\mathbf{s}$ is the correlated shadow fading experienced by all BSs; $g(PL_i S_i - \gamma \sum_{j\in\varphi/i} PL_j S_j)$ is a step function defined in (4.17).

$$g(PL_i S_i - \gamma \sum_{j\in\varphi/i} PL_j S_j) = \begin{cases} 1, & \text{when } PL_i S_i - \gamma \sum_{j\in\varphi/i} PL_j S_j < \frac{\gamma N_0}{P} \\ 0, & \text{when } PL_i S_i - \gamma \sum_{j\in\varphi/i} PL_j S_j > \frac{\gamma N_0}{P} \end{cases}. \tag{4.17}$$

Table 4.1: Simulation Configuration Parameters

Target Area	$1000m \times 1000m$
BS Densities	$3, 10, 50, 100, 200, 300, 500$
Path Loss Exponent	4
BS Transmission Power	$P : 40dbm$
SINR Requirement	$-5dB$
De-Correlation Distance	$20m, 200m$

4.5 Simulation Results

In this section, we present simulation setup and results. Firstly, we execute simulations to compare the outage probability of the two different network topologies: the Grid model and the Random model. Secondly, the SINR distribution and the outage probability of the Random model given different BS densities are investigated. Two scenarios are considered: MS connecting to the nearest BS and MS connecting to the BS providing highest SINR. At the end, the outage duration distribution is simulated and discussed given different BS densities. The simulation parameters are presented in Table 4.1.

Figure 4.4 shows the Cumulative Distribution Function (CDF) of SINR when the MS is connecting to the nearest BS. The de-correlation distance of the correlated shadow fading is $20m$. The figure suggests that the Grid model outperforms the Random model, which is consistent with findings in [57]. Figure 4.5 shows the outage probability with SINR threshold being $-5dB$. The outage probability of Grid model (blue) is lower than that of the Random model (yellow). In the next section, we will focus on the Random model, which is more realistic than the Grid model.

For the Random model, the SINR distribution and the outage probability of different BS densities are investigated for both the Nearest BS mode and the Strongest BS mode. Simulations are implemented under independent shadow

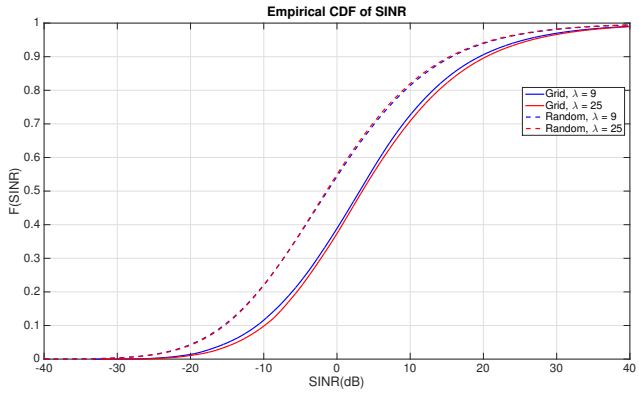

Figure 4.4: CDF of SINR given Grid model and Random model (de-correlation distance: $20m$)

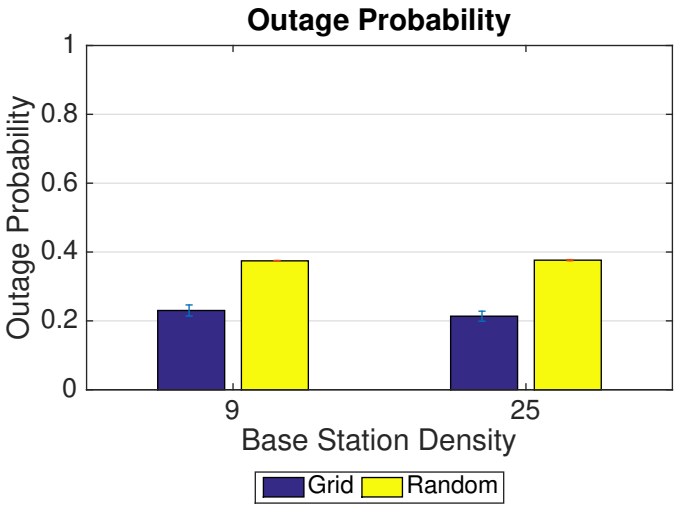

Figure 4.5: Outage probability given Grid model and Random model with $\gamma = -5dB$ (de-correlation distance: $20m$)

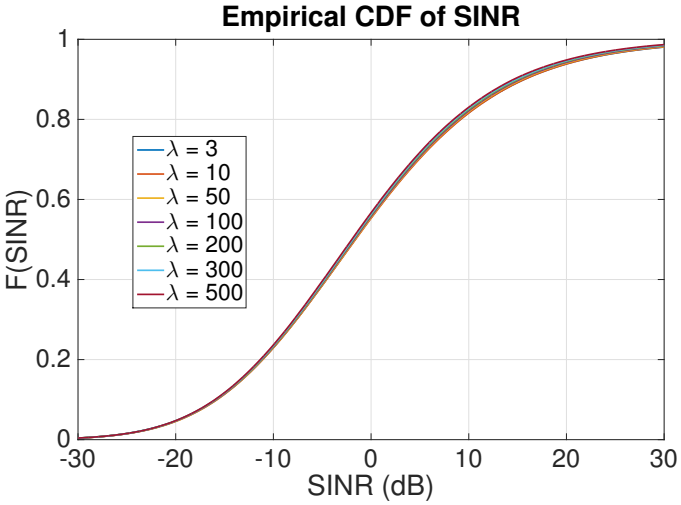

Figure 4.6: CDF of SINR (the MS is connecting to the nearest BS, independent shadow fading

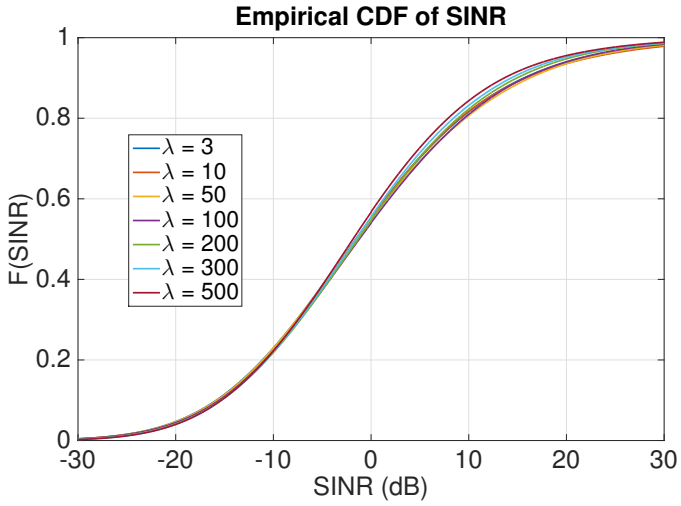

Figure 4.7: CDF of SINR (the MS is connecting to the nearest BS, correlated shadow fading with 20m de-correlation distance

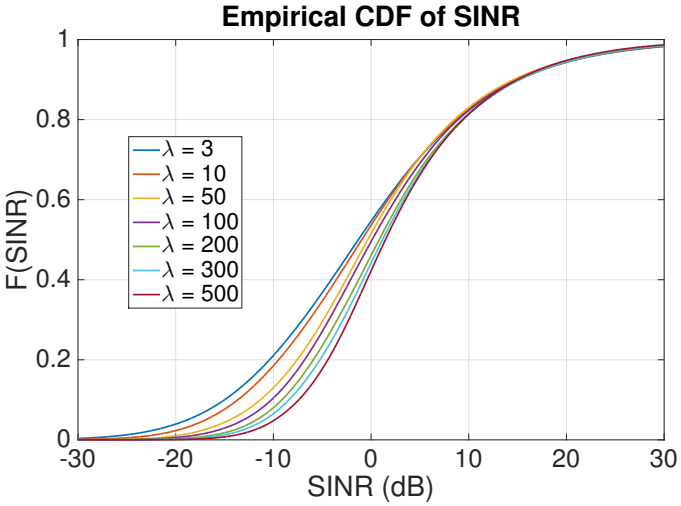

Figure 4.8: CDF of SINR (the MS is connecting to the nearest BS, correlated shadow fading with 200m de-correlation distance

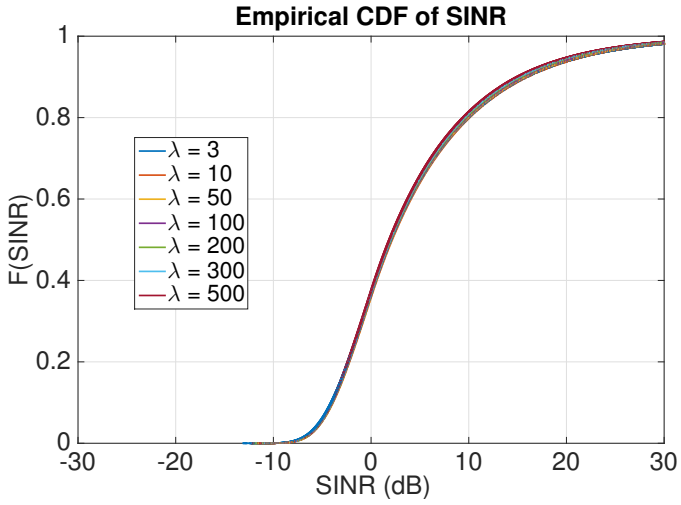

Figure 4.9: CDF of SINR (the MS is connecting to the strongest BS, independent shadow fading

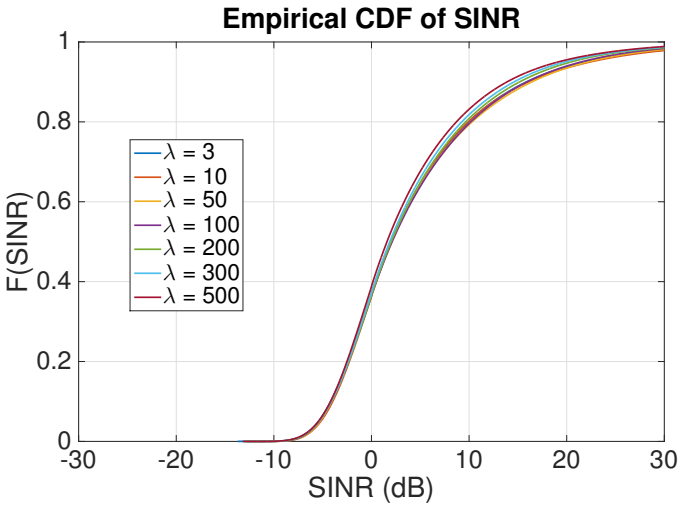

Figure 4.10: CDF of SINR (the MS is connecting to the strongest BS, correlated shadow fading with 20m de-correlation distance

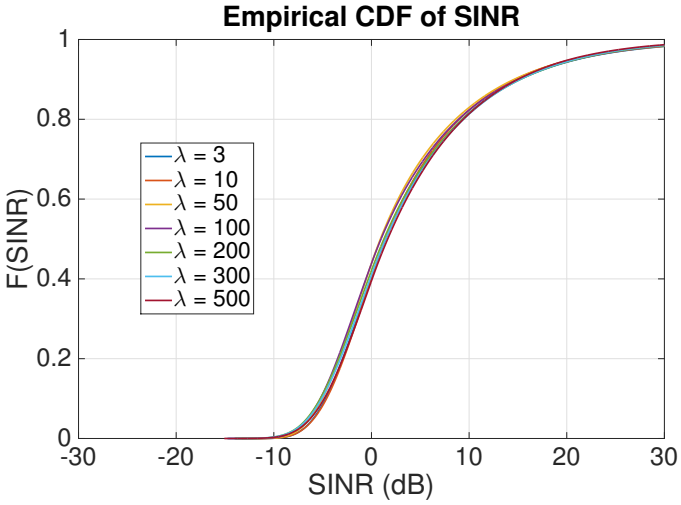

Figure 4.11: CDF of SINR (the MS is connecting to the strongest BS, correlated shadow fading with 200m de-correlation distance

fading and correlated shadow fading. CDF curves of SINR are generated and the outage probability given the SINR threshold being $-5dB$ are presented for increasing BS densities. Figure 4.6, 4.7 and 4.8 show the SINR of the MS when connecting to the nearest BS. From Figure 4.6 and 4.7, it is obvious that the CDF curves are overlapping each other, which means increasing BS density does not change the CDF of SINR. From this we can conclude, under the circumstance that the shadow fading is independent or the de-correlation distance of the correlated shadow fading is small, increasing the BS density will not improve the system performance in terms of reducing the outage probability. Figure 4.8 illustrates that CDF of SINR improves (curve moves toward the bottom-right corner) as we increase the BS density. Therefore, increasing the BS density will result in better system performance when the de-correlation distance is large, by reducing the outage probability. Figure 4.12 shows the outage probability of different correlated shadow fading models and different BS densities when SINR threshold is set to $-5dB$. These blue and green bars suggest that increasing the BS density will not decrease the outage probability when shadow fading is independent or correlated with $20m$ de-correlation distance. Meanwhile, these yellow bars suggest that when the de-correlation distance is $200m$, increasing the BS density will reduce the outage probability. For example, when the BS density is 3, the outage probability is around 38%. Increasing the BS density to 500, the outage probability decreases to 18%. Above simulation results suggest that when the de-correlation distance is relatively large and the MS is connecting to the nearest BS, increasing the BS density will reduce the outage probability and improve the system performance.

Next, we move forward to investigate the system performance when the MS chooses to connect to the BS, which provides the highest SINR. The same simulations as the nearest BS scenario are executed to explore this scenario. Figure

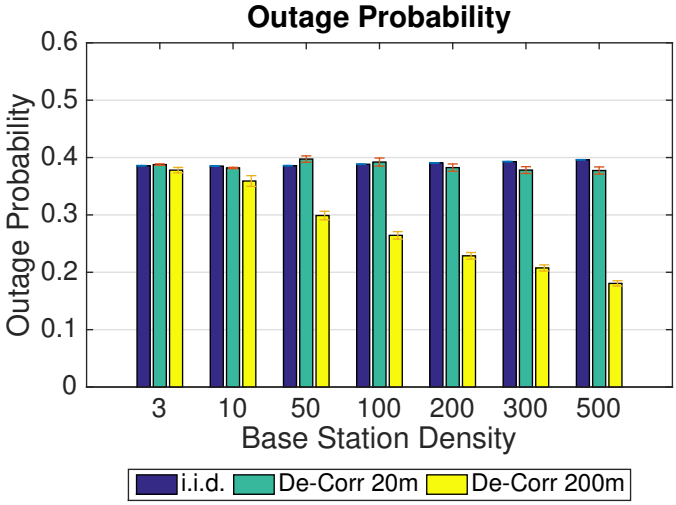

Figure 4.12: Outage probability given $-5dB$ SINR threshold

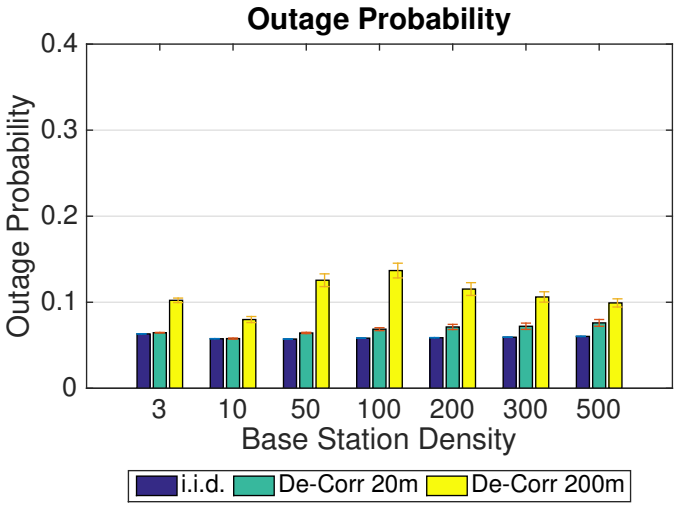

Figure 4.13: Outage probability given $-5dB$ SINR threshold

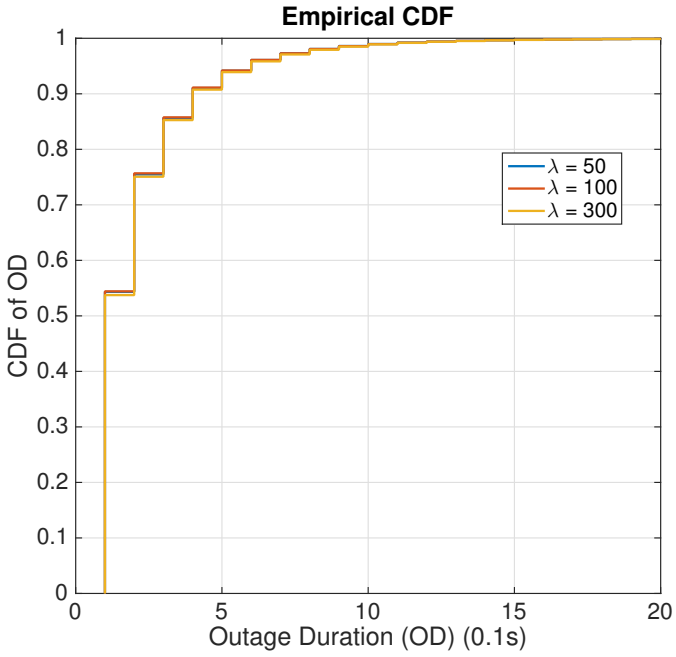

Figure 4.14: CDF of Outage Durations when the MS is connecting to the Nearest BS with independent shadow fading

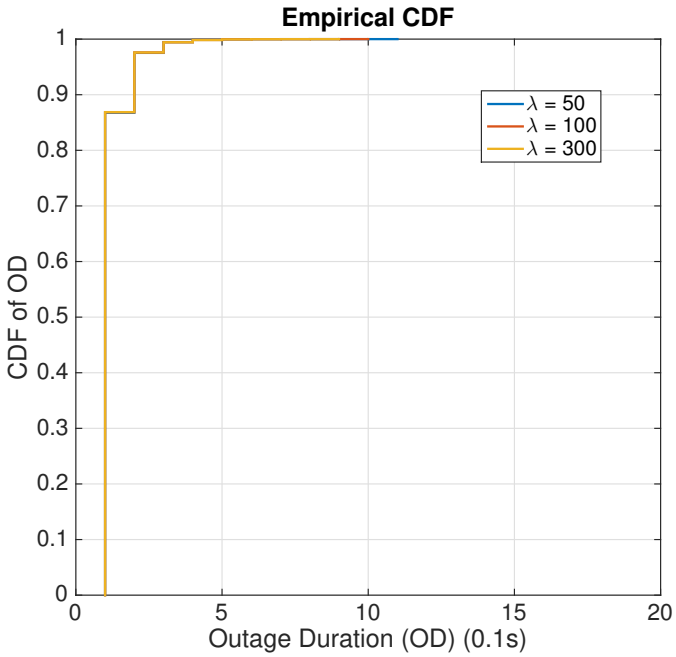

Figure 4.15: CDF of Outage Durations when the MS is connecting to the Strongest BS with independent shadow shadowing

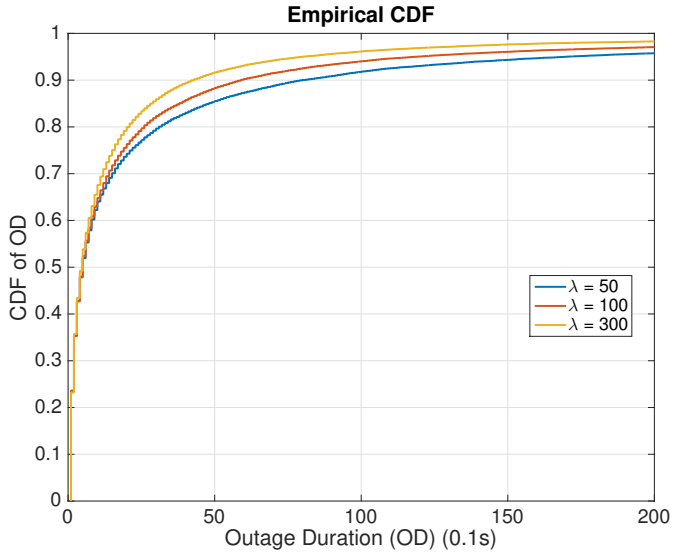

Figure 4.16: CDF of Outage Durations when MS is connecting to the Nearest BS with correlated shadowing (de-correlation distance: 200m)

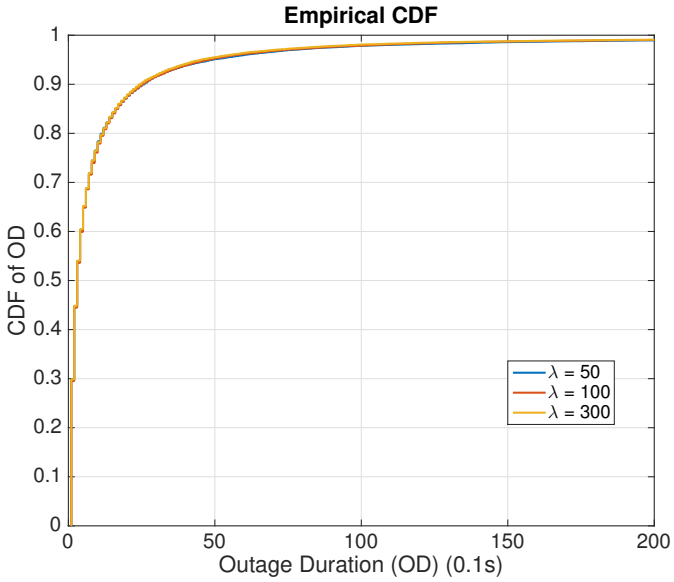

Figure 4.17: CDF of Outage Durations when MS is connecting to the Strongest BS with correlated shadowing (de-correlation distance: 200m)

4.9, 4.10 and 4.11 present the receiving SINR of the MS when connecting to the strongest BS. In Figure 4.9, 4.10 and 4.11, CDF curves of SINR almost overlap each other when increasing BS densities, which means increasing BS density will not change the CDF of SINR significantly. Figure 4.13 shows the outage probability bars, which are consistent with our conclusion. For each shadow fading model, the difference between the highest outage probability and the lowest outage probability is less than 5%. Comparing three different shadow fading models, we can conclude that when the MS is connecting to the strongest BS, long de-correlation distance will harm the system performance by increasing the outage probability (yellow bars are higher than green or blue bars).

Comparing Figure 4.12 with Figure 4.13, we find that with the same BS density, outage probabilities are lower for every shadow fading model if MS is connecting to the strongest BS. For example, with the independent shadow fading and the BS density being 50, the outage probability of the Nearest BS mode is 38%, while this probability of the Strongest BS mode is 6%. For correlated shadow fading with the de-correlation distance being $200m$ and the BS density being 50, we find that the outage probability of the Nearest BS mode is around 30%. This is higher than that of the Strongest BS mode, which is 14%. Therefore, we conclude that connecting to the BS which provides highest SINR will improve the system performance with regard to the same network setup.

In the end, we investigate the system performance from the perspective of outage duration. We use the Random Waypoint mobility model to model the user mobility. The parameters of the Random WayPoint model are given in Table 4.2. The MS speed is assumed to be between $1m/s$ (pedestrian speed) and $20m/s$ (highway car speed). The MS pause interval is assumed to be uniformly distributed between $0s$ to $60s$. The simulation time is set to be $0.1s$, which means

we check the MS's SINR every $0.1s$ to determine if it is in the outage area or not. Simulation results are shown in Figure 4.14, 4.16, 4.15 and 4.17. Comparing Figure 4.14 and Figure 4.16, Figure 4.15 and Figure 4.17, we conclude that when the channel is under independent shadow fading, the outage duration is usually less than $2s$. However, when the channel is under correlated shadow fading with $200m$ de-correlation distance, the outage duration can be longer than $20s$. Therefore, we draw the conclusion that correlated shadow fading leads to long-lasting outage durations and deteriorate the system performance. Comparing Figure 4.14 and Figure 4.15, we find that connecting to the strongest BS will reduce the outage duration. For example, the percentage of outage durations of the Nearest BS mode with a length less than $0.5s$ is 94%, while that of the Strongest BS mode is 100%. Figure 4.16 and Figure 4.17 confirm this conclusion in addition. For example, the percentage of outage durations less than $5s$ in Figure 4.16 is 85% with BS density being 50. However, this percentage in Figure 4.17 is increased to 95%. Furthermore, Figure 4.16 indicates that increasing the BS density will reduce the percentage of long-lasting outage durations if the MS is connecting to the nearest BS. For example, in Figure 4.16, when the BS density increases from 50 to 300, the percentage of outage durations longer than $5s$ is reduced from 15% to 8%. In contrast, for independent shadow fading and correlated shadow fading with the MS connecting to the strongest BS, increase the BS density will not change the distribution of outage durations, which is confirmed by Figure 4.14, Figure 4.15 and Figure 4.17. All CDF curves of outage durations are the same with different BS densities.

Table 4.2: Random Waypoint Mobility Model Parameters

Speed Interval	$1m/s - 20m/s$
Pause Interval	$0s - 60s$
Sample Time	$0.1s$

4.6 Chapter Summary

Shadow fading is a large-scale fading, which can cause significant received power loss for a wide area. In general, shadow fading is considered to be independent log-normal distributed to simplify the analysis; however, this is not the real case. In reality, shadow fading at two different positions are correlated to each other. Correlated shadow fading will result in correlated outage events and long-lasting outage durations. To investigate the performance of a multi-cell system given correlated shadow fading, simulations are implemented to analyze the outage probability and the outage duration distribution. First of all, the probability of two different BS layouts: Grid model and Random model are investigated. We find that the Grid model performs better than the Random model. Secondly, outage probabilities given different BS densities and two different connecting strategies: Nearest BS mode and Strongest BS mode, are simulated. We conclude that connecting to the strongest BS will reduce the outage probability compared with the nearest BS from simulation results. Increasing the BS density will not reduce the outage probability when the MS is connecting to the strongest BS. However, when the MS is connecting to the nearest BS and the de-correlation distance of correlated shadow fading is large enough, increasing the BS density will reduce the outage probability. Finally, we analyze the system performance in terms of outage duration. Simulation results show that correlated shadow fading will result in long-lasting outage durations. Simulation results show that increas-

ing the BS density will reduce the percentage of long-lasting outage durations if the MS chooses to connect to the nearest BS. Therefore, we suggest dense BS layout might be a proper strategy for next generation mmWave communication networks with correlated shadow fading.

Chapter 5

Transport Layer Protocols for Next Generation Networks

The rapid increase of smartphone use generates dramatical demand increase for capacity in mobile broadband communications every year. The wireless carriers and researchers are motivated to explore the underutilized millimeter wave (mmWave) frequency spectrum for next generation (Fifth Generation) broadband cellular communication networks. Fifth generation (5G) mmWave communication system will provide high speed, high capacity wireless communication networks to users. Meanwhile, mmWave channel is sensitive to obstructions, which results in frequent capacity fluctuations. Legacy transmission control protocols (TCP) might not work properly with the new channel; therefore, we first investigate the performance of legacy TCP on mmWave channel. Results indicate that mmWave channel requires a fast congestion detection scheme and an aggressive recovery scheme. Therefore, this chapter focuses on fast congestion detection scheme and presents a new end-to-end TCP congestion detection scheme for mmWave communication networks: Virtual Explicit Congestion Notification (Virtual ECN).

Virtual ECN leads to the flouring of the fast reacting congestion control protocol design.

5.1 Introduction

mmWave channel provides a tremendous amount of capacity and relatively low delay while suffering from high propagation loss and sensitivity to blockage. Simulations and measurements revealed that the capacity gain is significant, compared to current cellular systems [15, 16]. The last hop wireless channel capacity is no longer a bottleneck problem; meanwhile, mmWave channels are prone to variations due to the blockage from walls, trees or even human body [17–19]. This feature brings frequent capacity variations to the channel. Typically, the channel switches periodically between Line-of-Sight (LOS) and Non-Line-of-Sight (NLOS). The upper layer channel provided by mmWave communication network is not yet standardized. But in general, there is a consensus that mmWave channel will provide high capacity and low latency with frequent capacity fluctuations. For mmWave wireless communication networks, the legacy TCP congestion control might not work well due to the slow congestion detection and conservative loss recovery. Our investigation on legacy TCP with emulated mmWave channel confirms this. Therefore, designing a new TCP congestion control scheme without involving any intermediate network device is necessary. In this chapter, we will illustrate the initial step to design such a scheme: develop an end-to-end fast data-driven congestion detection algorithm.

In recent years, several promising TCP congestion control protocols have been developed such as BIC TCP [60], CUBIC TCP [28], Compound TCP [61] and so on. Most of these TCP congestion control schemes rely on three duplicate ACKs

or Retransmission Timeout to detect the congestion and packet loss. This means TCP needs to wait for at least three Round-Trip-Time (RTT) or a retransmission timeout before entering into recovery mode or slow start mode. The slow congestion detection will deteriorate the network performance for a high capacity, low latency mmWave channel with frequent capacity variations. First, more congestion and packet loss might occur during this interval and cause high payoff to recover from the loss for a high capacity link. Secondly, for a network with capacity variations, the slow congestion detection scheme might provide out of date information of the congestion status, which makes the TCP congestion control protocol extremely conservative.

This chapter is organized as follows: Section 5.2 explains the related work on TCP congestion control and mmWave channel. Motivations to design this scheme is demonstrated in this section. In section 5.3, we investigate the legacy TCP congestion control performance on anemulated emulated mmWave channel for both NewReno and Cubic. Section 5.4 demonstrates the proposed fast end-to-end congestion detection scheme in detail including network simulation setup, data process and congestion prediction. Section 5.5 summarizes the chapter and proposes future work, which can be accomplished based on this scheme.

5.2 Related Work

In this section, we present the related work on mmWave channel modeling and data-driven TCP congestion control.

5.2.1 mmWave Channel

In [62] [63], research on the feasibility of using mmWave to provide wireless communication service is presented. In [15], researchers investigated the mmWave propagation loss, penetration loss, interference and provided a detailed statistical mmWave channel model based on outdoor measurement. This model elaborates that mmWave system can provide an order of magnitude increase in capacity. In addition, the probabilities of outage and non-outage were demonstrated. Coverage design technology and beam-forming scheme are discussed in [64] [65], which convince us that mmWave can be used for future wireless communication network design. Although mmWave channel can provide high capacity and low latency, it has a challenging issue: mmWave is sensitive to obstructions like buildings, trees and even nearby pedestrians or vehicles. These obstructions may cause sudden, short and severe channel downgrade. How to increase the reaction speed to the channel fluctuations and fully utilize the channel capacity is the main issue for TCP congestion control protocol design. This chapter focuses on solving this problem from an end-user perspective.

5.2.2 Explicit Congestion Notification (ECN)

Legacy TCP congestion control protocols consider duplicate ACKs as an indication of packet loss. With the addition of active queue management and ECN [30] to the network infrastructure, routers are capable of detecting congestion before queue overflows. An additional Congestion Experienced (CE) byte is added to the IP header of the packet to support this function. Routers running RED queue management can mark the CE code point with a certain probability when the average queue length is between minimal threshold and maximal threshold. When

the average queue length exceeds the maximal threshold, upcoming packets' CE byte will be marked with probability 1. The packet with marked CE will be sent to the receiver. After receiving the packet, the receiver will piggyback an ACK with marked CE to notify the sender that there is congestion in the router. No extra traffic will be generated to overload the network. The sender will reduce the congestion window to avoid queue overflow and packet loss. Using ECN to detect congestion requires the participation of routers and waiting for receiver's feedback. We develop an end-user congestion prediction scheme that utilizes the idea of ECN without involving any network devices or waiting for any feedback.

5.2.3 Remy

Remy [66] was proposed by Keith Winstein in 2013. It is a congestion-control scheme based on prior knowledge of the network and the traffic model. It is the first computer generated congestion control protocol. A RemyCC tracks only three state variables of the end-user:

- An exponentially weighted moving average (EWMA) of the inter-arrival time between new ACKs received (ack_ewma).
- An EWMA of the time between TCP sender timestamps reflected in those ACKs (send_ewma).
- The ratio between the most recent Round Trip Time (RTT) and the minimum RTT during the current connection (rtt_ratio).

The algorithm does not require the support from any intermediate network devices. The end-user can adjust its sending speed following the pre-generated

algorithm based on the above mentioned data. This indicates that these three variables together might reflect the congestion state of the network.

Remy convinces us that designing a data-driven congestion detection algorithm using end-user data is possible. Since ECN provides accurate information of whether there is congestion in the network or not, we decide to use end-user data to predict ECN, thereby detecting the congestion. The main contribution of this chapter is developing a data-driven fast congestion detection algorithm (within one ACK inter-arrival time) using end-user data without support from receivers, routers or other network devices.

5.3 Legacy TCP Performance on Emulated 5G Channel

Since Ethernet has a similar capacity with mmWave channel, we use Ethernet with periodic on-off behavior to emulate mmWave channel. On period means the channel is in the state of LOS while off period means the channel is in the NLOS state. We test two existing TCP congestion control protocols: NewReno and Cubic on the emulated mmWave channel. In GENI Portal, a three-node line topology with a server, a middle box and a client was set up as in Figure 5.1. Two different kinds of channel behavior are investigated: uniformly distributed on-off period and exponentially distributed on-off period. Congestion window size (CWND) and throughput are recorded to analyze the performance as in Figure 5.2, 5.3, 5.4 and 5.5. The channel capacity is set to be 1Gbps. Figure 5.2 illustrates the CWND of the sender when the off period is exponentially distributed with mean $10ms$, $100ms$, $1s$, while Figure 5.3 shows the corresponding throughput.

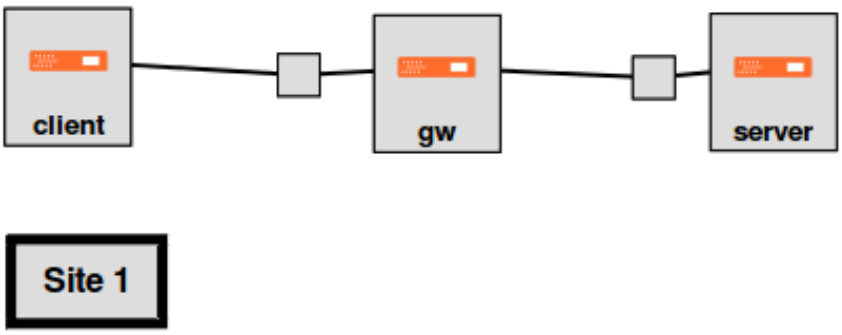

Figure 5.1: GENI Topology for Performance Evaluation

Figure 5.4 and 5.5 presents the CWND and throughput when the off period is uniformly distributed between $0ms-10ms$, $0ms-100ms$, $0ms-1s$. In both cases, NewReno performance is deteriorated significantly due to the high frequency of off period. Figure 5.2 and 5.4 demonstrate that slow start will be initiated after every off period. The throughput is as low as 200Mbps, which is 20% of the full capacity. Comparing with NewReno, from Figure 5.2 and 5.4 we conclude that Cubic is more aggressive than NewReno. When a channel recovers from off period to on period, Cubic will increase the CWND faster to utilize the channel capacity. When channel off time is at the level of 10ms, cubic did not even notice there is a connection drop. Instead, it behaves as congestion happened in the network and reduces the CWND. Whenever the on time period is long enough as in the exponentially on-off period case, Cubic can still reach the upper limit of CWND and achieve full throughput as in Figure 5.3, while NewReno needs more time to recover. In uniformly distributed on-off period case, the channel lost occurred before Cubic fully recovered as in Figure 5.4. The CWND has a descending trend and the throughput decreases as time goes on. Based on the aforementioned observation, we conclude that even Cubic will not achieve high

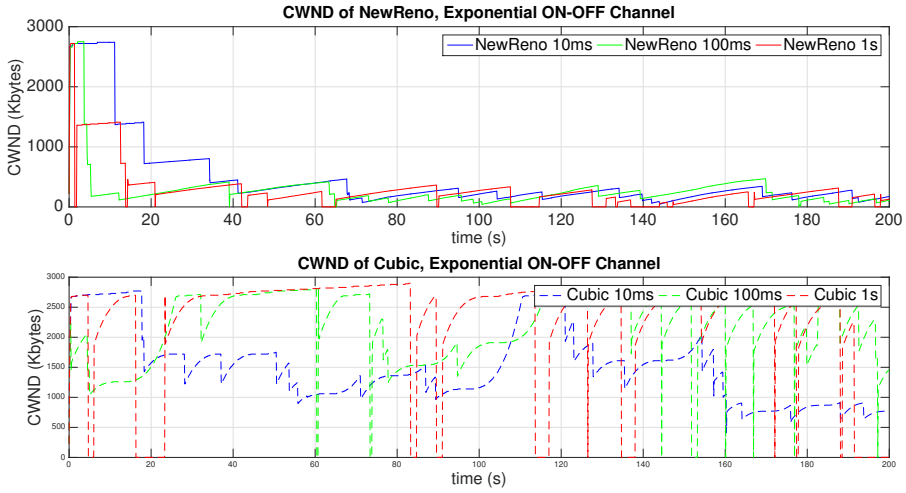

Figure 5.2: CWND dynamics given exponentially On-Off channel behavior

throughput if the channel switch between LOS (on) and NLOS (off) with a high frequency. Therefore, an aggressive congestion control protocol is necessary for the next generation networks. In the following sections, we will focus on the initial step of design this protocol: developing a fast end-user congestion prediction scheme.

5.4 Congestion Detection Algorithm

The design of the fast congestion detection algorithm is illustrated in detail in this section. The principle idea is to predict the congestion in network within one inter-arrival time of ACKs from end-user data. Data which can be collected from the end-user includes packet sending time, ACK arriving time and the RTT calculated from these two timestamps. We run simulations using discrete event-based Network Simulator 2 (NS2) to collect theses data for a particular network topology.

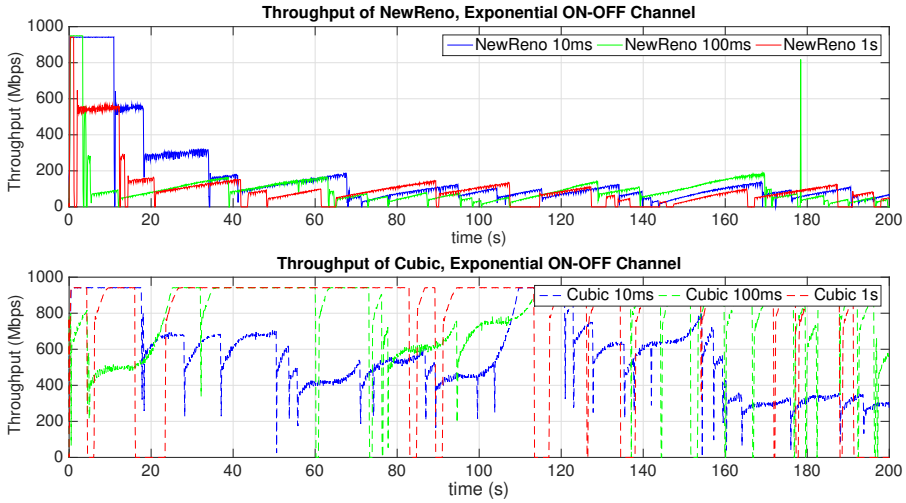

Figure 5.3: Throughput dynamics given exponentially On-Off channel behavior

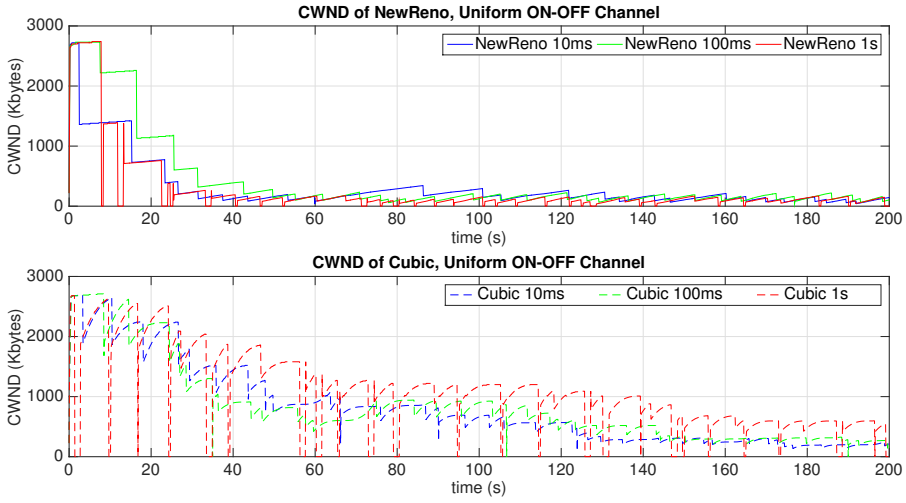

Figure 5.4: CWND dynamics given uniformly On-Off channel behavior

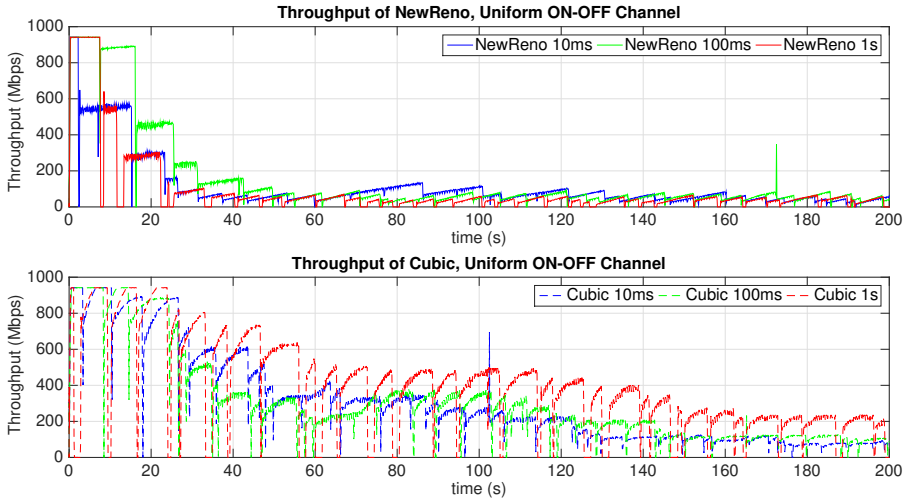

Figure 5.5: Throughput dynamics given uniformly On-Off channel behavior

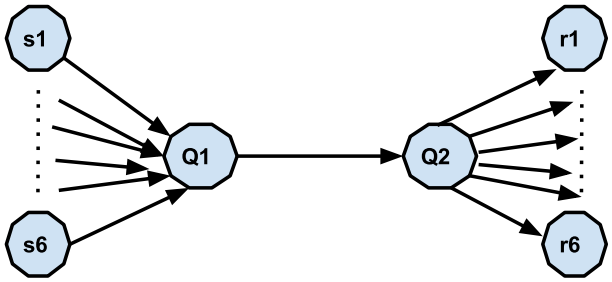

Figure 5.6: Network topology

5.4.1 Network Topology

A typical dumbbell model is presented and used in this section. The network topology is shown in Figure 5.6. There are 6 TCP traffic senders and 6 receivers; the sender s_i sends data to receiver r_i through the bottleneck link $Q1 \rightarrow Q2$. Both $Q1$ and $Q2$ maintain a DropTail Queue. The queue limit is set to be the bandwidth-delay product to ensure the full utilization of the link capacity.

Congestion occurs when the occupied queue length exceeds the threshold T on the arriving of the incoming packet. To generate traces with congestion identifiers,

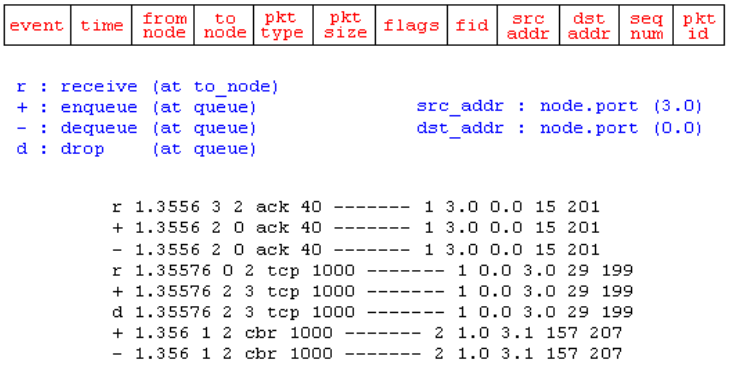

Figure 5.7: NS2 TCP trace format

we mark every packet as Congestion Experienced in the queue when queue length is greater than T. Typical NS2 TCP traces [67] are collected for future data processing as in Figure 5.7.

From the trace format, we can identify the packet sending time, arriving time, packet size, unique ID, etc. Matching the packet unique ID, RTT can be calculated from packet sending time and corresponding ACK receiving time. For each unique packet, if congestion happens upon its arriving, the unique ID will be recorded to be Congestion Experienced.

The drop tail queue behavior is displayed as follows. Figure 5.8 shows queue changes when traffic sources are running Cubic TCP with UDP competing traffic. In this case, when queue length is greater than 450 packets, the incoming packets will be marked as congestion experienced.

5.4.2 Data Collection

Without losing of generality, we simulated several different traffic scenarios to collect end-user data. We analyze the following scenarios:

- Scenario 1: All traffic sources are running TCP NewReno with stationary

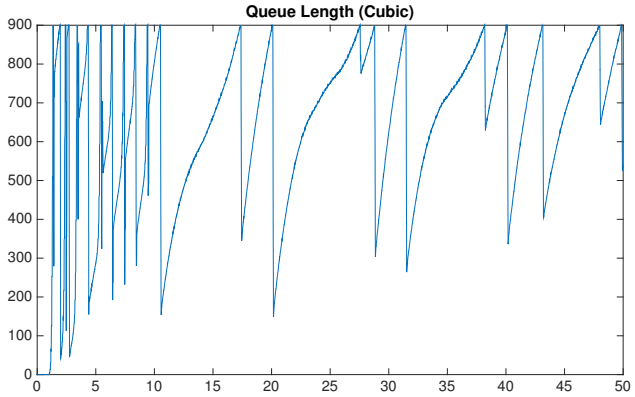

Figure 5.8: Queue length dynamics (Cubic)

bottleneck link capacity.

- Scenario 2: All traffic sources are running TCP Cubic with stationary bottleneck link capacity.
- Scenario 3: One-half of the traffic sources is running TCP NewReno while the other half is running UDP with stationary bottleneck link capacity.
- Scenario 4: One-half of traffic sources is running TCP Cubic while the other half is running UDP with stationary bottleneck link capacity.
- Scenario 5: Repeat scenario 1 and 2 for a periodically On-Off bottleneck link.

The bottleneck link for those scenarios is link $Q1 \rightarrow Q2$. Detailed simulation parameters are shown in Table 5.1.

Data available from end-user includes packet sending time t_s and ACK receiving time t_r. From these two timestamps, we can calculate packet sending interval $T_{s_i} = t_{s_i} - t_{s_{i-1}}$, ACK inter-arrival time $T_{r_i} = t_{r_i} - t_{r_{i-1}}$ and Round Trip Time (RTT) $RTT_i = t_{s_i} - t_{r_i}$. From the above three available time intervals, we develop 5 features that are used in the congestion prediction algorithm.

Table 5.1: Simulation Parameters

Access Link Capacity	1Gbps
BottleNeck Link Capacity	1Gbps
Access Link Delay	5ms
BottleNeck Link Delay	10ms
Queue Capacity	Bandwidth-Delay Product

- Sending time interval between two consecutive packets T_{s_i}.
- Receiving time interval between two consecutive ACKs T_{r_i}.
- An exponentially-weighted moving average (EWMA) of T_{s_i} (send_ewma).
- An EWMA of T_{r_i} (ack_ewma).
- The ratio between the most recent RTT and the minimum RTT during the entire connection period (rtt_ratio).

These above five features construct the feature set to train the machine learning algorithm and predict congestions.

5.4.3 Congestion Prediction

Every sample of the data collected from above five scenarios includes five features and a congestion identifier: Virtual ECN (0 represents non congestion experienced, 1 represents congestion experienced). The problem to be solved is a binary classification problem: train an algorithm to classify the sample data into two categories: congestion experienced and non congestion experienced. First, we apply Logistic Regression, a popular binary classification algorithm, to train the sample data and predict congestions. The area under ROC curve is 0.89 as shown in Figure 5.9. The performance of Logistic Regression is good $(0.80 - 0.90)$. The

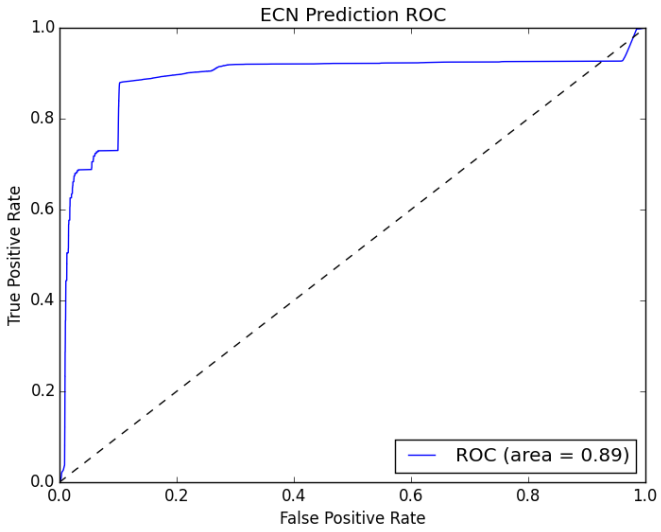

Figure 5.9: ROC curve of Logistic Regression classifier

decision boundary is $-2.32*f_1-33.36*f_2-12.65*f_3-15.30*f_4+2.03*f_5-2.69=0$, where f_1, f_2, f_3, f_4, f_5 are the five corresponding features.

Next, we applied Decision Tree algorithm and regulated the maximum depth of the tree to be 5 and the minimum samples in each leaf node to be 10000 to avoid overfitting. Figure 5.10a presents the ROC curve of Decision Tree Classifier. The area under ROC curve is 0.98. This indicates excellent (area under ROC: $0.90-1$) prediction result. The feature importance is given as [0.011703, 0.00085, 0.000000, 0.03985, 0.94760] for [T_{s_i}, T_{r_i}, send_ewma, receive_ewma, rtt_ratio], from which we can conclude that rtt_ratio is the most important feature to predict congestions.

Furthermore, we changed the maximum depth to 3 and minimum samples of each leaf node to $100,000$, the ROC is displayed in Figure 5.10b. The feature importance turns to [0, 0, 0, 0, 1]. This indicates the decision tree is doing the binary classification merely based on rtt_ratio. All other features do not contribute to the binary classification process at all. The decision tree is shown in

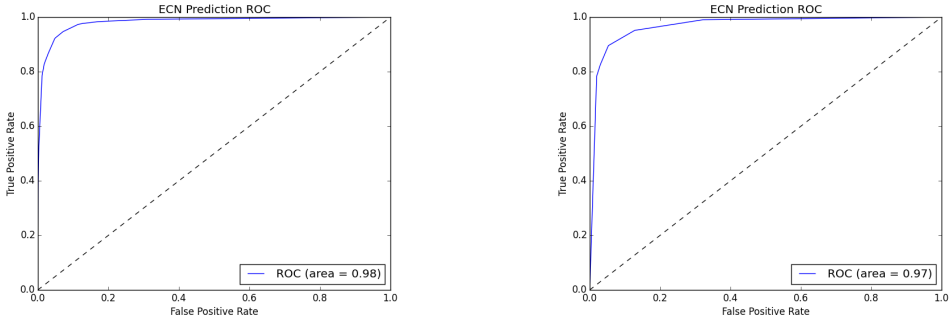

(a) max_depth = 5, min_samples_leaf = 10000

(b) max_depth = 3, min_samples_leaf = 100000

Figure 5.10: ROC curve of Decision Tree classifier

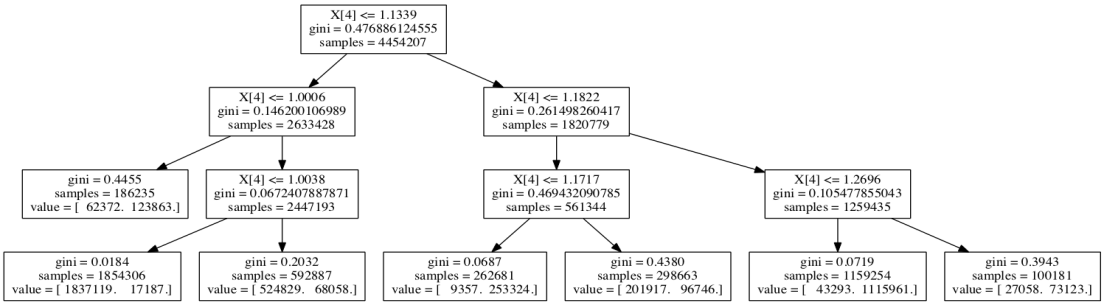

Figure 5.11: Decision Tree (max_depth = 3, min_samples_leaf = 100000)

Figure 5.11. In this figure, the first layer is classified by X[4] which is rtt_ratio. The cumulative density function (CDF) of rtt_ratio is given in Figure 5.12a. The blue line is the CDF curve of rtt_ratio when congestion is experienced while the red line is the CDF curve when congestion is not experienced. Take rtt_ratio = 1.2 as an example, the probability of rtt_ratio to be less than 1.13 is 82% when there is no congestion. However, this probability is approximately 0% when congestion experienced. This is consistent with the result of feature importance generated from Decision Tree algorithm.

The above results are generated from a network with fixed propagation delay. To learn how this prediction algorithm works when network condition changes, we investigate Scenario 1 and 2 with variations of propagation delay. We simulate

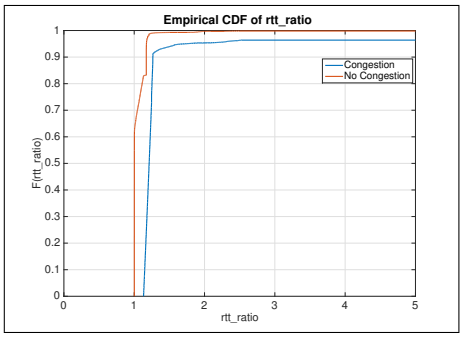

(a) CDF of rtt_ratio with same propagation delay

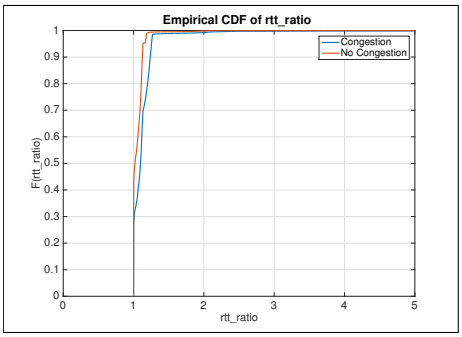

(b) CDF of rtt_ratio with different propagation delay

Figure 5.12: CDF of rtt_ratio

Table 5.2: Simulation Parameters

Access Link Delay	5ms, 10ms, 20ms
BottleNeck Link Delay	10ms, 20ms, 40ms
Queue Capacity	Bandwidth-Delay Product

networks with access delay and queue capacity as in Table 5.2. The Logistic Regression algorithm generates ROC curve which is shown in Figure a. The area under ROC curve is 0.65, which indicates poor performance (area under ROC curve: $0.60-0.70$). The decision boundary is $-0.47*f_1-7.33*f_2-0.35*f_3-1.41*f_4+5.20*f_5-5.54=0$. The coefficient of each feature follows the same pattern as before. Decision Tree classifier is then applied to the collected dataset. The ROC curve is shown in Figure. b. The area under ROC curve is 0.70, which is on the boundary of poor performance. The feature importance is [0.000955787581, 0.000389816495, 0.00489484823, 0.0636899225, 0.930069625]. This is consistent with the previous result that rtt_ratio is the most important feature. Those two figures indicate that when network condition changes, the predictability of congestion from the aforementioned five features decreases. Figure. 5.12b shows the CDF of rtt_ratio with different link propagation delay. The figure indicates near 30% overlap between CDF curves of Congestion Experience packet and No

Congestion packet. This again verifies the prediction results.

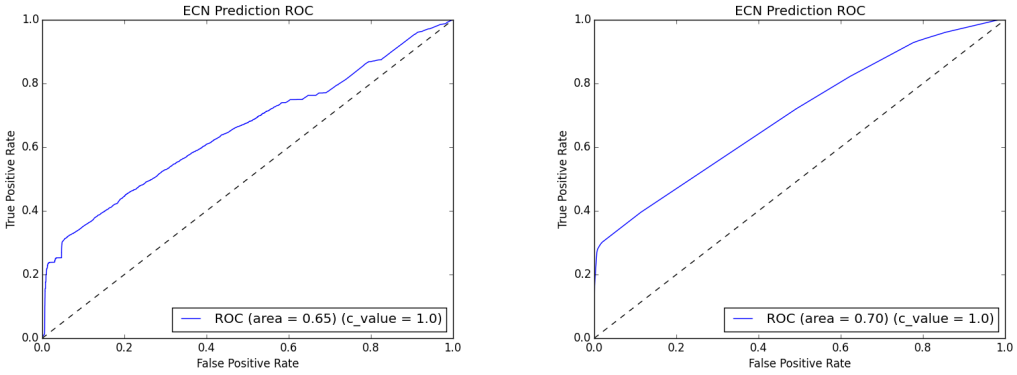

(a) ROC curve of Logistic Regression classifier with different propagation delay

(b) ROC curve of Decision Tree classifier with different propagation delay

Figure 5.13: ROC curves with different propagation delay

5.5 Chapter Summary

In this chapter, we proposed a data-driven machine learning congestion detection algorithm. Datasets are collected using NS2 for a dumbbell model with five different traffic scenarios. Five features are formatted from end-user data. When the network condition is not changing, which means the propagation delay of each link is stable, our algorithm can detect congestion with high precision from those five features. In contrast, if the network condition changes, the algorithm fails to work. In both cases, rtt_ratio is the most important feature to predict congestion. The other four features are less useful when doing the binary classification. CDF of rtt_ratio explains our conclusion. For stable network, a fast reacting congestion control algorithm can be designed based on our congestion detection algorithm for mmWave communication networks.

Chapter 6

Conclusion

Appendices

Appendix A

A.1 Title of Appendix A

Appendix B

B.1 Title of Appendix B

Bibliography

[1] C. V. N. Index, "Global mobile data traffic forecast update, 2012-2017," *Cisco white paper*, 2013.

[2] P. Cerwall and S. Bergqvist, "Ericsson traffic and market data report [r]," *Ericsson, Stockholm, Sweden, Nov*, 2011.

[3] F. Pujol, "?mobile traffic forecasts 2010-2020 & offloading solutions," *IDATE Consulting and Research, May*, vol. 15, 2011.

[4] F. Khan and Z. Pi, "mmwave mobile broadband (mmb): Unleashing the 3–300ghz spectrum," in *Sarnoff Symposium, 2011 34th IEEE*. IEEE, 2011, pp. 1–6.

[5] Z. Pi and F. Khan, "An introduction to millimeter-wave mobile broadband systems," *IEEE Communications Magazine*, vol. 49, no. 6, 2011.

[6] T. S. Rappaport, J. N. Murdock, and F. Gutierrez, "State of the art in 60-ghz integrated circuits and systems for wireless communications," *Proceedings of the IEEE*, vol. 99, no. 8, pp. 1390–1436, 2011.

[7] P. Pietraski, D. Britz, A. Roy, R. Pragada, and G. Charlton, "Millimeter wave and terahertz communications: Feasibility and challenges," *ZTE Communications*, vol. 10, no. 4, pp. 3–12, 2012.

[8] S. Rangan, T. S. Rappaport, and E. Erkip, "Millimeter-wave cellular wireless networks: Potentials and challenges," *Proceedings of the IEEE*, vol. 102, no. 3, pp. 366–385, 2014.

[9] C. H. Doan, S. Emami, D. A. Sobel, A. M. Niknejad, and R. W. Brodersen, "Design considerations for 60 ghz cmos radios," *IEEE Communications Magazine*, vol. 42, no. 12, pp. 132–140, 2004.

[10] Y. P. Zhang and D. Liu, "Antenna-on-chip and antenna-in-package solutions to highly integrated millimeter-wave devices for wireless communications," *IEEE Transactions on Antennas and Propagation*, vol. 57, no. 10, pp. 2830–2841, 2009.

[11] F. Gutierrez, S. Agarwal, K. Parrish, and T. S. Rappaport, "On-chip integrated antenna structures in cmos for 60 ghz wpan systems," *IEEE Journal on Selected Areas in Communications*, vol. 27, no. 8, 2009.

[12] S. Rajagopal, S. Abu-Surra, Z. Pi, and F. Khan, "Antenna array design for multi-gbps mmwave mobile broadband communication," in *Global Telecommunications Conference (GLOBECOM 2011), 2011 IEEE*. IEEE, 2011, pp. 1–6.

[13] S. S. Szyszkowicz, H. Yanikomeroglu, and J. S. Thompson, "On the feasibility of wireless shadowing correlation models," *Vehicular Technology, IEEE Transactions on*, vol. 59, no. 9, pp. 4222–4236, 2010.

[14] M. Gudmundson, "Correlation model for shadow fading in mobile radio systems," *Electronics Letters*, vol. 27, no. 23, pp. 2145–2146, 1991.

[15] M. R. Akdeniz, Y. Liu, M. K. Samimi, S. Sun, S. Rangan, T. S. Rappaport, and E. Erkip, "Millimeter wave channel modeling and cellular capacity evaluation," *Selected Areas in Communications, IEEE Journal on*, vol. 32, no. 6, pp. 1164–1179, 2014.

[16] T. Bai and R. W. Heath, "Coverage and rate analysis for millimeter-wave cellular networks," *Wireless Communications, IEEE Transactions on*, vol. 14, no. 2, pp. 1100–1114, 2015.

[17] J. Lu, D. Steinbach, P. Cabrol, and P. Pietraski, "Modeling the impact of human blockers in millimeter wave radio links," *ZTE Commun. Mag*, vol. 10, no. 4, pp. 23–28, 2012.

[18] H. Zhao, R. Mayzus, S. Sun, M. Samimi, J. K. Schulz, Y. Azar, K. Wang, G. N. Wong, F. Gutierrez, and T. S. Rappaport, "28 ghz millimeter wave cellular communication measurements for reflection and penetration loss in and around buildings in new york city," in *Communications (ICC), 2013 IEEE International Conference on*. IEEE, 2013, pp. 5163–5167.

[19] A. V. Alejos, M. G. Sánchez, and I. Cuiñas, "Measurement and analysis of propagation mechanisms at 40 ghz: Viability of site shielding forced by obstacles," *Vehicular Technology, IEEE Transactions on*, vol. 57, no. 6, pp. 3369–3380, 2008.

[20] A. Goldsmith, *Wireless Communications*. Cambridge University Press, 2005.

[21] V. Graziano, "Propagation correlations at 900 MHz," *Vehicular Technology, IEEE Transactions on*, vol. 27, no. 4, pp. 182–189, 1978.

[22] M. Marsan, G. Hess, and S. Gilbert, "Shadowing variability in an urban land mobile environment at 900 mhz," *Electronics Letters*, vol. 26, no. 10, pp. 646–648, 1990.

[23] J. C. Liberti and T. S. Rappaport, "Statistics of shadowing in indoor radio channels at 900 and 1900 mhz," in *Military Communications Conference, 1992. MILCOM'92, Conference Record. Communications-Fusing Command, Control and Intelligence., IEEE*. IEEE, 1992, pp. 1066–1070.

[24] D. Kitchener, M. Naden, W. Tong, P. Zhu, G. Senarnath, H. Zhang, D. Steer, and D. Yu, "Correlated lognormal shadowing model," *San Diego, CA, IEEE*, vol. 802, 2006.

[25] S. S. Szyszkowicz, "Interference from large wireless networks under correlated shadowing," Ph.D. dissertation, Carleton University, 2011.

[26] S. S. Panwar, *TCP/IP Essentials: A Lab-Based Approach*. Cambridge University Press, 2004.

[27] L. A. Grieco and S. Mascolo, "Performance evaluation and comparison of westwood+, new reno, and vegas tcp congestion control," *ACM SIGCOMM Computer Communication Review*, vol. 34, no. 2, pp. 25–38, 2004.

[28] S. Ha, I. Rhee, and L. Xu, "Cubic: a new tcp-friendly high-speed tcp variant," *ACM SIGOPS Operating Systems Review*, vol. 42, no. 5, pp. 64–74, 2008.

[29] D. Lin and R. Morris, "Dynamics of random early detection," in *ACM SIGCOMM Computer Communication Review*, vol. 27, no. 4. ACM, 1997, pp. 127–137.

[30] K. Ramakrishnan, S. Floyd, and D. Black, "Rfc 3168," *The addition of Explicit Congestion Notification (ECN) to IP. The Internet Society*, 2001.

[31] T. S. Rappaport, *Wireless Communications: Principles and Practice*. Prentice Hall PTR New Jersey, 1996.

[32] F. Fabbri and R. Verdone, "The impact of correlated channel fluctuations on the connectivity of wireless ad-hoc networks," in *Vehicular Technology Conference, 2009. VTC Spring 2009. IEEE 69th.* IEEE, 2009, pp. 1–5.

[33] N. Patwari and P. Agrawal, "Effects of correlated shadowing: Connectivity, localization, and rf tomography," in *Information Processing in Sensor Networks, 2008. IPSN'08. International Conference on.* IEEE, 2008, pp. 82–93.

[34] M.-K. Chang and S.-Y. Lee, "Performance analysis of cooperative communication system with hierarchical modulation over rayleigh fading channel," *Wireless Communications, IEEE Transactions on*, vol. 8, no. 6, pp. 2848–2852, 2009.

[35] Y. Lee and M.-H. Tsai, "Performance of decode-and-forward cooperative communications over nakagami-fading channels," *Vehicular Technology, IEEE Transactions on*, vol. 58, no. 3, pp. 1218–1228, 2009.

[36] R. Madan, N. B. Mehta, A. F. Molisch, and J. Zhang, "Energy-efficient cooperative relaying over fading channels with simple relay selection," *Wireless Communications, IEEE Transactions on*, vol. 7, no. 8, pp. 3013–3025, 2008.

[37] V. Emamian, P. Anghel, and M. Kaveh, "Multi-user spatial diversity in a shadow-fading environment," in *Vehicular Technology Conference, 2002. Proceedings. VTC 2002-Fall. 2002 IEEE 56th*, vol. 1. IEEE, 2002, pp. 573–576.

[38] B. Kasiri, M. Naderi, and B. Abolhassani, "A new realistic relay selection method based on correlated shadowing for multihop cellular networks," in *Computer and Electrical Engineering, 2008. ICCEE 2008. International Conference on.* IEEE, 2008, pp. 669–673.

[39] S. Park and W. Stark, "Opportunistic relaying in multipath and slow fading channel: Relay selection and optimal relay selection period," in *Military Communications Conference, 2011-MILCOM 2011.* IEEE, 2011, pp. 661–666.

[40] A. Bletsas, H. Shin, M. Z. Win *et al.*, "Outage-optimal cooperative communications with regenerative relays," in *Information Sciences and Systems, 2006 40th Annual Conference on.* IEEE, 2006, pp. 632–637.

[41] N. Zlatanov, R. Schober, Z. Hadzi-Velkov, and G. Karagiannidis, "Average outage and non-outage duration of selective decode-and-forward relaying," in *Information Theory (CWIT), 2011 12th Canadian Workshop on.* IEEE, 2011, pp. 94–97.

[42] D. Kaltakis, M. A. Imran, and R. Hoshyar, "Uplink capacity with correlated lognormal shadow fading," in *Vehicular Technology Conference, 2009. VTC Spring 2009. IEEE 69th.* IEEE, 2009, pp. 1–5.

[43] A. Nosratinia, T. E. Hunter, and A. Hedayat, "Cooperative communication in wireless networks," *Communications Magazine, IEEE*, vol. 42, no. 10, pp. 74–80, 2004.

[44] S. Saunders and A. Aragón-Zavala, *Antennas and propagation for wireless communication systems.* John Wiley & Sons, 2007.

[45] Y. Zhang, J. Zhang, D. Dong, X. Nie, G. Liu, and P. Zhang, "A novel spatial autocorrelation model of shadow fading in urban macro environments," in *Global Telecommunications Conference, 2008. IEEE GLOBECOM 2008. IEEE.* IEEE, 2008, pp. 1–5.

[46] T. B. Sorensen, "Correlation model for slow fading in a small urban macro cell," in *Personal, Indoor and Mobile Radio Communications, 1998. The Ninth IEEE International Symposium on*, vol. 3. IEEE, 1998, pp. 1161–1165.

[47] J. Weitzen and T. J. Lowe, "Measurement of angular and distance correlation properties of log-normal shadowing at 1900 MHz and its application to design of PCS systems," *Vehicular Technology, IEEE Transactions on*, vol. 51, no. 2, pp. 265–273, 2002.

[48] H. L. Bertoni, *Radio Propagation for Modern Wireless Systems.* Pearson Education, 1999.

[49] W. W.-S. Wei, *Time Series Analysis.* Addison-Wesley Publ, 1994.

[50] A. Papoulis and S. U. Pillai, *Probability, Random Variables, and Stochastic Processes.* McGraw-Hill Higher Education, 2002.

[51] A. A. Abu-Dayya and N. C. Beaulieu, "Outage probabilities of cellular mobile radio systems with multiple nakagami interferers," *Vehicular Technology, IEEE Transactions on*, vol. 40, no. 4, pp. 757–768, 1991.

[52] I. Petrovic, M. Stefanovic, P. Spalevic, S. R. Panic, and D. Stefanovic, "Outage analysis of selection diversity over rayleigh fading channels with multiple

co-channel interferers," *Telecommunication Systems*, vol. 52, no. 1, pp. 39–50, 2013.

[53] V. Emamian, "Outage analysis of a multi-user spatial diversity system in a shadow-fade propagating channel," *British Journal of Applied Science & Technology*, vol. 4, no. 1, p. 40, 2014.

[54] M. Vural, G. K. Kurt, and C. Schneider, "The effect of shadow fading distributions on outage probability and coverage area," in *Vehicular Technology Conference (VTC Spring), 2015 IEEE 81st.* IEEE, 2015, pp. 1–6.

[55] T. Lu, P. Liu, and S. S. Panwar, "How long before i regain my signal?" in *Information Sciences and Systems (CISS), 2015 49th Annual Conference on.* IEEE, 2015, pp. 1–5.

[56] T. Lu, P. Liu, and S. Panwar, "Shining a light into the darkness: How cooperative relay communication mitigates correlated shadow fading," in *Vehicular Technology Conference (VTC Spring), 2015 IEEE 81st.* IEEE, 2015, pp. 1–7.

[57] J. G. Andrews, F. Baccelli, and R. K. Ganti, "A tractable approach to coverage and rate in cellular networks," *Communications, IEEE Transactions on*, vol. 59, no. 11, pp. 3122–3134, 2011.

[58] C. S. Chen, V. M. Nguyen, and L. Thomas, "On small cell network deployment: A comparative study of random and grid topologies," in *Vehicular Technology Conference (VTC Fall), 2012 IEEE.* IEEE, 2012, pp. 1–5.

[59] S. Kumar, "Approximate outage probability and capacity for-shadowed fading," *Wireless Communications Letters, IEEE*, vol. 4, no. 3, pp. 301–304, 2015.

[60] L. Xu, K. Harfoush, and I. Rhee, "Binary increase congestion control (bic) for fast long-distance networks," in *INFOCOM 2004. Twenty-third AnnualJoint Conference of the IEEE Computer and Communications Societies*, vol. 4. IEEE, 2004, pp. 2514–2524.

[61] K. Tan, J. Song, Q. Zhang, and M. Sridharan, "A compound tcp approach for high-speed and long distance networks," in *Proceedings-IEEE INFOCOM*, 2006.

[62] Y. Niu, Y. Li, D. Jin, L. Su, and A. V. Vasilakos, "A survey of millimeter wave communications (mmwave) for 5g: opportunities and challenges," *Wireless Networks*, pp. 1–20, 2015.

[63] T. S. Rappaport, S. Sun, R. Mayzus, H. Zhao, Y. Azar, K. Wang, G. N. Wong, J. K. Schulz, M. Samimi, and F. Gutierrez, "Millimeter wave mobile communications for 5g cellular: It will work!" *Access, IEEE*, vol. 1, pp. 335–349, 2013.

[64] S. Sun, G. R. MacCartney, M. K. Samimi, S. Nie, and T. S. Rappaport, "Millimeter wave multi-beam antenna combining for 5g cellular link improvement in new york city," in *Communications (ICC), 2014 IEEE International Conference on.* IEEE, 2014, pp. 5468–5473.

[65] W. Roh, J.-Y. Seol, J. Park, B. Lee, J. Lee, Y. Kim, J. Cho, K. Cheun, and F. Aryanfar, "Millimeter-wave beamforming as an enabling technology

for 5g cellular communications: theoretical feasibility and prototype results," *Communications Magazine, IEEE*, vol. 52, no. 2, pp. 106–113, 2014.

[66] K. Winstein and H. Balakrishnan, "Tcp ex machina: Computer-generated congestion control," in *ACM SIGCOMM Computer Communication Review*, vol. 43, no. 4. ACM, 2013, pp. 123–134.

[67] "Trace analysis example," http://nile.wpi.edu/NS/analysis.html, accessed: 2016-4-5.